Numerical Analysis of Electromagnetic Convection for Single Crystal SiC Growth by Top Seeded Solution Growth (TSSG) Technique

by

İmdat Emirhan Özcan
B.Sc., YILDIZ TECHNICAL UNIVERSITY, 2018

A Thesis Submitted in Partial Fulfillment of the
Requirements for the Degree of

MASTER OF APPLIED SCIENCE

in the Department of Mechanical Engineering

Numerical Analysis of Electromagnetic Convection for Single Crystal SiC Growth by Top Seeded Solution Growth (TSSG) Technique

by

İmdat Emirhan Özcan
B.Sc., YILDIZ TECHNICAL UNIVERSITY, 2018

Supervisory Committee

Dr. Rodney Herring, Supervisor
(Department of Mechanical Engineering)

Dr. Peter Oshkai, Unit Member
(Department of Mechanical Engineering)

Abstract

Top-Seeded Solution Growth (TSSG) is a very effective single crystal growth process that is working based on the Czochralski method. In this growth technique, there is a seed crystal that is dipped into the melt of the same material at a high temperature. It has a boundary between the seed crystal and melt where growth occurs. This boundary is highly affected by the fluid flow. Controlling the fluid flow is the key feature of the TSSG technique. Many advanced materials can be obtained by this method. Silicon Carbide (SiC) studied in this thesis is one of the advanced materials that shows semiconductor properties. Because of this attribute, SiC is widely used in the electronics industry.

In this thesis, different convection mechanisms are investigated for SiC single-crystal growth with the TSSG technique. Since the graphite crucible is the only source of carbon atoms in the system, transportation of carbon atoms from the crucible walls to the seed crystal is needed for efficient growth. To maintain this transportation, the silicon melt is induction coupled by electromagnetic coils. Controlling the fluid flow is maintained with electromagnetic forces which are generated by the coils in the TSSG furnace. Respectively, a numerical study has been conducted to determine the electromagnetic forces in the silicon melt. Also, the distribution of electromagnetic forces in the silicon melt is analyzed. Effects of different working frequencies are described. Results are compared to the buoyancy body forces in the system. To overcome buoyancy forces in the system, the needed amount of electromagnetic forces is explained.

Contents

List of Figures

Chapter 1

Introduction

Single crystal solution growth is an essential technique for advanced materials production that can be used in many areas today such as computer industry, aviation sector or the defense industry. Silicon Carbide (SiC) is a very strategic semiconductor material because of its high temperature resistance and high thermal conductivity. This single crystal material is widely used in the electronics applications such as computer chips. In order to grow better single crystal SiC material, this study focuses on the Top-Seeded Solution Growth (TSSG) technique. The first chapter starts with defining the research objective. Then, it gives brief information about the crystal growth technology and its history.

1.1 Research Objective

This thesis focuses on a numerical simulation of the fluid flow during Top-Seeded Solution Growth (TSSG) process of the Silicon Carbide (SiC). The simulation is carried out to determine electromagnetic body force that induced by TSSG furnace. Effects of the electromagnetic force are analyzed. The outcome is compared with the buoyancy body forces which is generated by the temperature difference in the system. The simulation is repeated many times to find optimal working frequency of the coils that generates higher electromagnetic body forces with the uniform distribution. This optimal frequency is needed to make the fluid flow controlled by electromagnetic convection rather than buoyancy convection in the silicon melt which can be used to grow single SiC crystal with the TSSG technique.

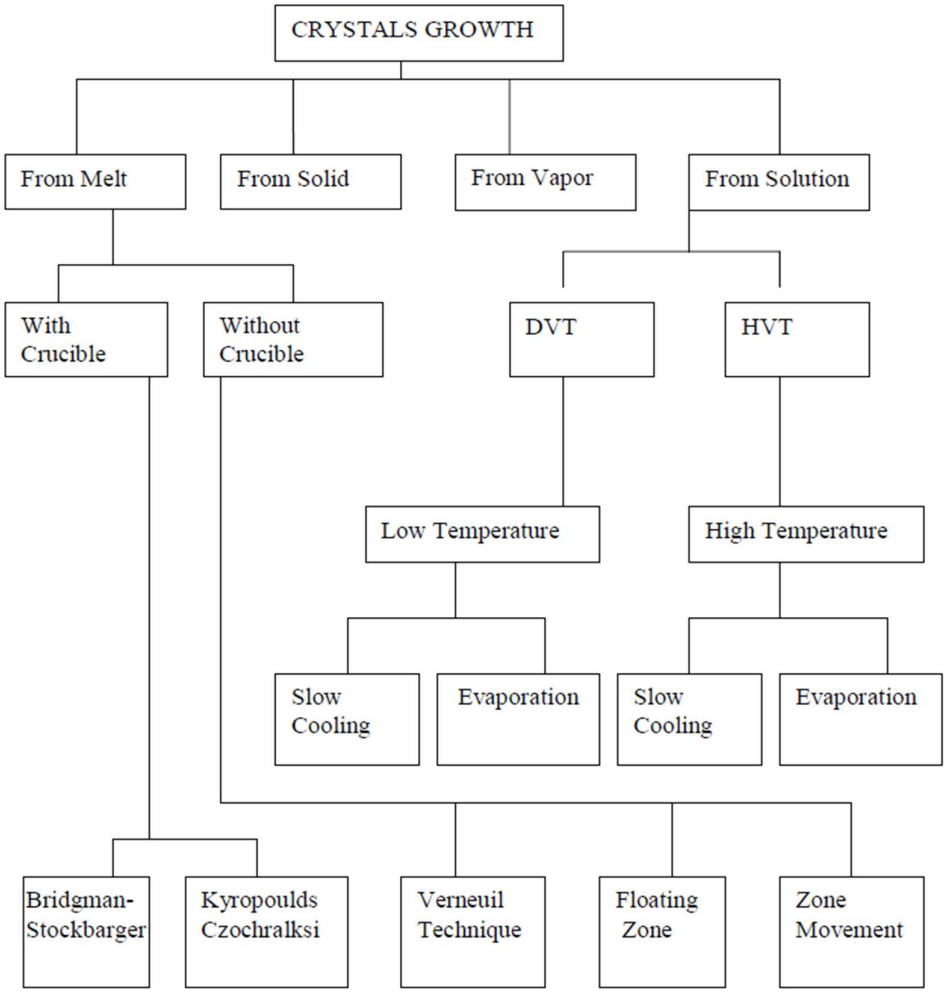

Figure 1.1: Brief Classification of Crystal Growth Methods [2]

1.2 History of Crystal Growth Technology

Production of crystal growth at an industrial scale is considered to begin with the French Chemist A. Verneuil. He invented the flame fusion growth method. He was melting the powdered material with oxyhydrogen flame and maintaining crystallization from the droplets of melt into a boule [9]. He was using nucleation control and crystal-diameter control principles. This is considered the first time to control these two mechanisms during crystal growth [3]. These principles are later being used by other growth from melt methods, like Bridgman Method and Czochralski Method.

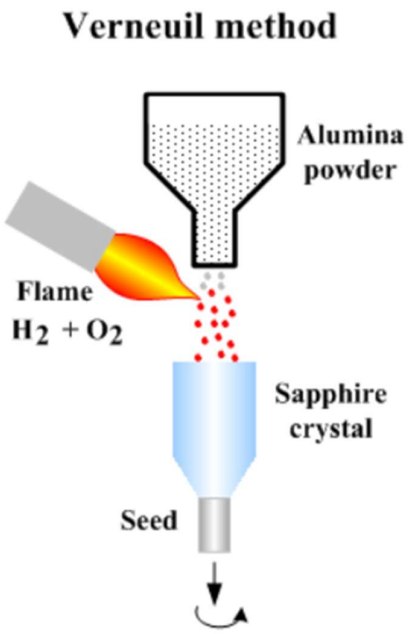

Figure 1.2: A simple schematic for Verneuil Method (Flame Fusion Method)

1.3 Czochralski method

Based on principles like growth rate, nucleation, and diameter control, The polish scientist,-Jan Czochralski invented this method. It starts with a seed crystal touching the melt in a crucible. Then, the seed is pulled at a predetermined rate [13].

Czochralski method is widely used on semiconducting materials for mainly commercial reasons. Also, this method has the advantage that crystals are not constrained to the shape of the crucible. The working principle of the Czochralski method is to increase melted material's temperature slightly above the melting point [12]. Since the pulling rod has a lower temperature than melt, when the rod is pulled slowly the tip of the rod collects the crystal. The rate of pulling varies with different factors such as latent heat of fusion of charge, rate of cooling, and thermal conductivity. At the same time, the seed is rotated to keep the crystal uniform and cylindrical.

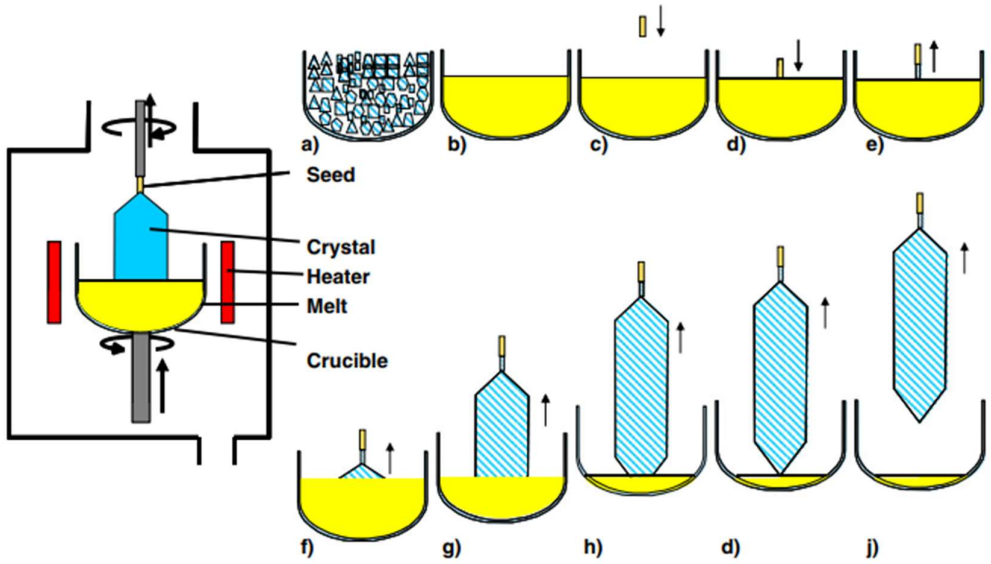

Figure 1.3: Schematic of the principle of the Czochralski method (left) and illustration of the different steps (a–j) of the Cz process for growing a Si crystal [10].

However, despite its old age, this still remains one of the most important methods for the fabrication of semiconductor and oxide crystals consisting of pulling crystals from melts contained in crucibles.

Advantages

- Used to grow large single crystals and used frequently in the semiconductor industry
- Since there is no direct contact with the crucible and crystal, it produces an unstressed single crystal (it is also a cause of can process of large and well-defined crystals with the Czochralski Method)

Disadvantage

- Generally, this method needs synthetic research before using. Using incongruently may alter results.

1.4 Bridgman (Bridgman–Stockbarger) Method

The Bridgman technique was named after their inventors Bridgman and Stockbarger (1925 and 1938 respectively). The method is heating polycrystalline material above its melting temperature and slowly cooling liquid to the end of the container where the seed crystal is located [11]. Single crystal material is formed based on the diameter and volume of the container. This process can be completed horizontally or vertically.

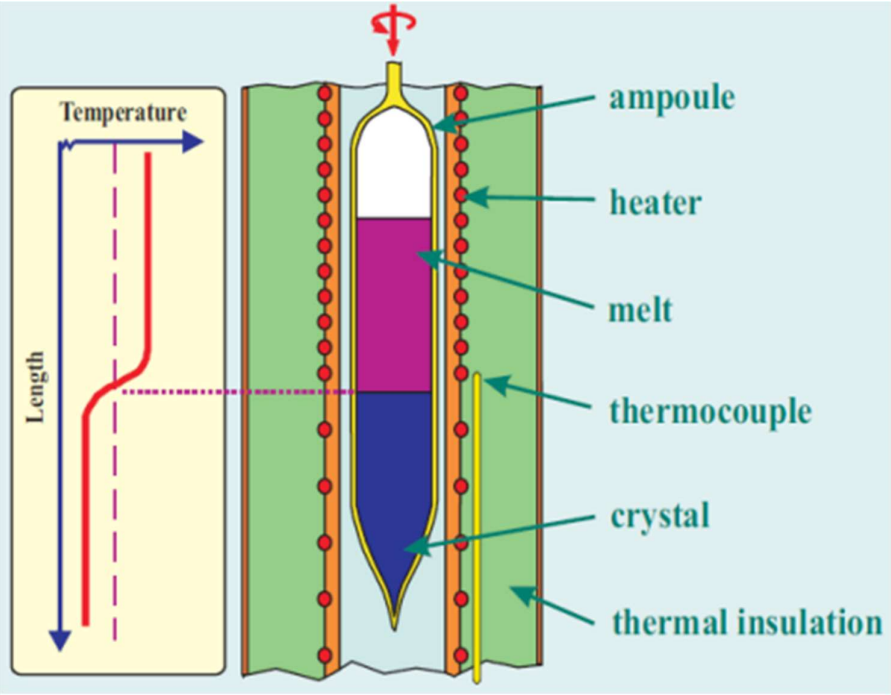

Figure 1.4: Bridgman-Stockbarger Method [4]

Advantages

- Bridgman Method is one of the simplest methods and is relatively very low cost.
- If a convenient container is selected, a crystal with a pre-assigned diameter can be produced.

Disadvantage

- Internal high stresses can be developed inside due to compression of the solid. In the material, this may be high enough to create new dislocation

Chapter 2

Solution Growth

This chapter investigates solution growth and its techniques. To have better understanding on the Top-Seeded Crystal Growth technique, some other crystal growth techniques are briefly explained. Also, the solution growth mechanism is explained. There are a comparison of low temperature and high temperature solution growth methods. At the end of the chapter, there are more information about the Top-Seeded Crystal Growth technique and there is an example furnace in Fig 2.5. Finally, the chapter is concluded with the silicon-carbide phase diagram.

2.1 Mechanism

Starting from the melt, crystal growth requires first-order phase transitions. In the phase diagram, two distinct uniform phases must exist at the equilibrium point and be divided by a phase boundary-like interface. Near the equilibrium borders, one of them will be in a thermodynamically stable phase meanwhile the other one is in a metastable phase. The metastable phase will be supercooled. Consequently, this will increase the driving force of crystallization which is needed for the spontaneous nucleation of the crystal [10]. Starting from the seed crystal and slowly pulling the crystal from the melt, has been considered a very effective way of controlling single-crystal growth.

Substances should be crystallized from supersaturated solutions [11]. These conditions must be merged with nonreactive solvents that are fairly soluble and referred to as a solution on crystal growth techniques together. These nonreactive solvents can be formed from water, various organic liquids, some chemical compounds, and their mixtures. Although water and organic liquids are in the liquid state in the laboratory environment, other chemicals to be used can generally become in the liquid state at higher temperatures. When considering usable solvent types, the main differentiation is that of low and high-temperature solutions. For the low-temperature solutions in crystal growth systems, the crystallization temperature is usually below 80 °C. For the high-temperature solutions in crystal growth systems, the crystallization temperature is usually below 1300 °C [1]. In both these applications, the maximum possible growth temperature is the boiling point of the solvent.

2.2 Low Temperature Solution Growth

The low-temperature solutions may be more effective on the crystal growth if materials decompose in the melt at higher temperatures and undergo structural transformations while cooling from higher temperatures [14]. It also allows for the build of different morphologic and polymorphic formed monocrystals due to the low-temperature advantage. In addition, materials have a variety from micrometer-sized crystalline organic chemicals to large inorganic nonlinear optical crystals. Low-temperature solution growth has mainly three advantages. The first one is growth apparatus is simple and cheap this causes used widely in industry. Secondly, when using low temperatures for melts, crystals are exposed to relatively low thermal stress, equilibrium defects, and dislocations [10]. It allows to the growth of more uniform crystals with more simple solution mixtures relative to high-temperature solution growth systems. Finally, since the low-temperature crystals have a uniform and measurable growth curves, it provides convenient post-calculations and observation of foundation like an in-situ observation of surfaces and capture of impurities.

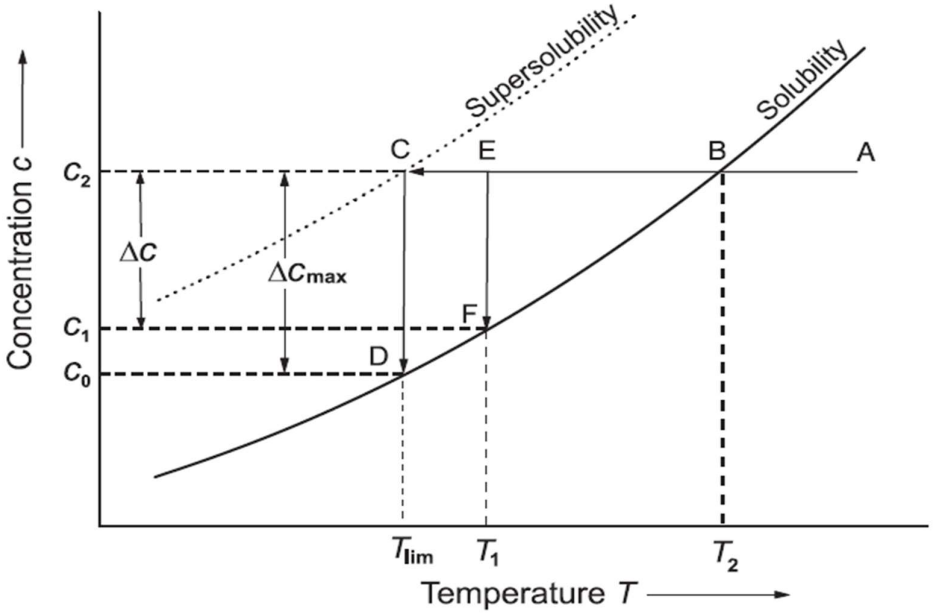

Figure 2.1: Supersolubility and Solubility Curves [5]

T_{lim}, if the concentration is lower than c_0, the solution is in the "Stable Undersaturated Zone". In addition to that, if we define Figure 5 to a temperature/concentration function as a F (T,c); The Unstable Supersaturated Zone is above the super solubility curve. For example, when the temperature is T_{lim}, the concentration is more than c_2 that represented in that zone as well.

The Metastable Zone is labeled as between the solubility curve and super solubility curve. According to the function definition above, F $(T_{lim}, c_0 +)$, F (T_{lim}, c_1), F $(T_{lim}, c_2 -)$, and F $(T_1, c_1 +)$, F (T_1, c_2) are all on the metastable zone. The process of spontaneous nucleation and crystal growth only occurs in that zone thus demanding that solution should be at that saturation level to better satisfy growth conditions [5].

2.3 High-Temperature Solution Growth

The growth from melt was a convenient method for specific compounds, however since complex multicomponent compounds have a high melting point, high vapor pressure, and high decomposing, the melting only can be the solution at relatively huge temperatures. Because of that problem, complex compounds can be mono-crystallized at lower temperatures than melting points with high-temperature solutions [10]. In this method, the first component is dissolved in a solvent at a high temperature. To obtain crystallization in a high-temperature solution, supersaturation should be achieved similarly to the low-temperature solution growth methods [1]. Supersaturated solutions can be attained from various techniques. For example, slow-cooling of the solution is used for crystal growth or evaporation of solvent to form a nucleate in solutions. Also creates a temperature difference between the growth apparatus and the solution. High-temperature solution growth can be carried out in air or a suitable environment [1].

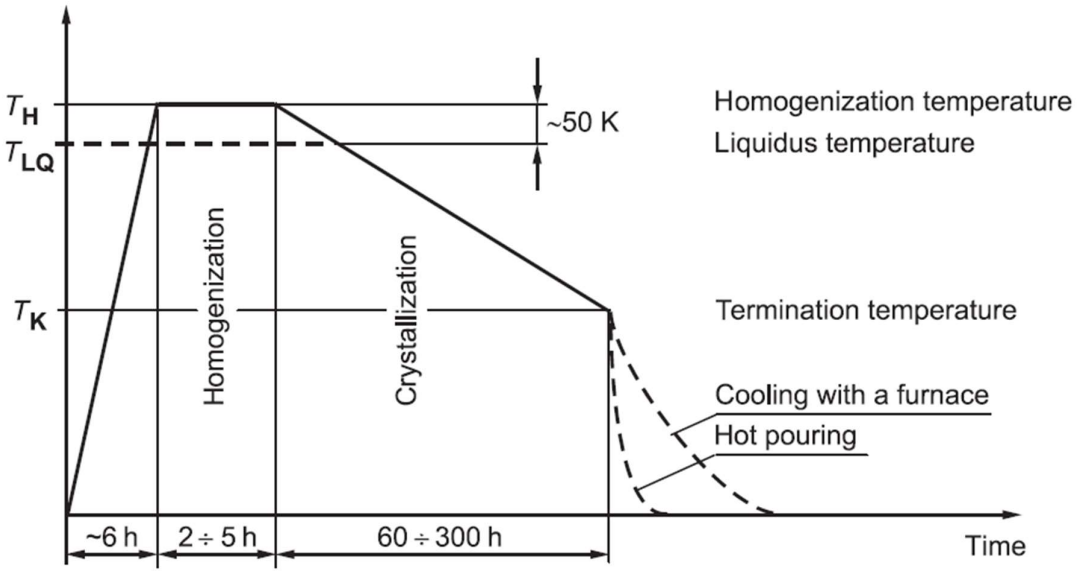

Figure 2.2: Typical procedure for crystal growth from high-temperature solutions [5]

2.4 Composition of Fluxes and Their Selection

In the high-temperature solution growth technique, the selection of a suitable solvent and its physical and chemical properties are crucial parts and hugely related to our output monocrystal. At the growth temperature, the solvent should be in the metastable zone to satisfy the required solubility of components. Solvents also must ensure sufficient solubility change related to temperature increase or decrease [16]. Also, the solvent should have a low melting point, low volatility, low viscosity, and low toxicity. The crystallized compound should be in stable form when mixed with the solvent [15]. Furthermore, the solvent should be available and cheap in a pure state and does not corrode the growth apparatus, the crucible, or the furnace.

Crystal	Solvent/Solution	Method
KTP	$K_8P_6O_{19}$–BaF_2	Top-seeded solution growth; Pt crucible, homogenization at 1100 °C, cooled at 40 °C/h to about 900 °C, seed introduced at about 10 °C above saturation temperature, te
KTP:Zr	K_2O–P_2O_5–TiO_2–ZrF_4	Slow cooling method; Pt crucibles, homogenization at 1100 °C for 10 h, cooled to 750 °C at 3 K/h
NdP_5O_{14}	$H_2P_4O_7$	Slow solvent evaporation; platinum crucible, growth temperature 500 °C
$KNbO_3$	K_2CO_3–NbO_5	Micropulling down; Pt crucible, cooling rate 30 °C/min, pulling rate 0.5 mm/min
$LaMn_{1-x}Co_xO_3$	Cs_2MoO_4–MoO_3	Electrochemical growth; Pt crucible, anode current density 5–10 mA/cm^2, 80–100 h
$LiNbO_3$	(Li_2O:Nb_2O_5)–K_2O	Czochralski method; pulling rate 2 mm/h, rotation rate 20 rpm
3C-SiC	Si	Top-seeded dipping method (LPE); graphite crucible, growth on dipping 6H-SiC(0001) seed mounted at the end of graphite rod at 1300 °C for 50 h

Figure 2.3: Some examples of single crystals grown by different methods [1].

2.5 Crystal Growth Techniques

As stated before, achieving a supersaturated solution is one of the main objectives for crystal growth. There are three different techniques that satisfy this objective and further grow the crystal. These are temperature reduction (Slow-Cooling Method), solvent evaporation, and temperature gradient methods. In these techniques, supersaturated solvent is attained by the cooling rate of the solvent, the solvent evaporation rate, and the temperature difference between saturated and growth zones, respectively [14].

2.6 Slow-Cooling Method

This method is relatively simple to run and has low requirements for finances and know-how. Used growth apparatus is simple, conventional muffle furnaces and small crucibles usually sufficient. Also, a growth run requires relatively low attention after the beginning. Generally used for producing small crystals.

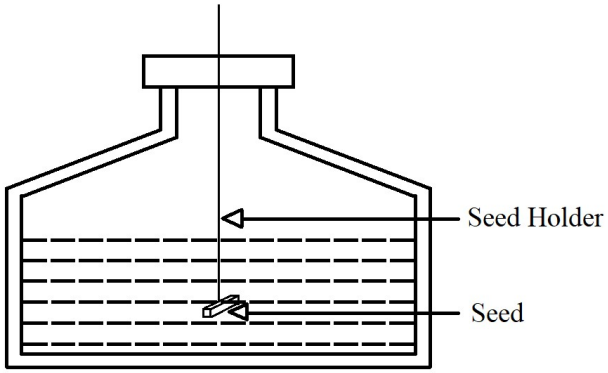

Figure 2.4: Slow-Cooling approach

There are two main difficulties with the slow cooling technique, the amount of strain in the crystal and high nucleation density. Strain is caused by different thermal expansion coefficients and high nucleation is caused by the small size of crystals mainly [15]. Strain can be relatively normalized by draining away the flux before the start of fast cooling. High nucleation density can be solved by using small temperature oscillations at the nucleation stage of blowing a stream of cold air in a localized small region.

2.7 Basic Features of TSSG Technique

In the temperature gradient methods, the solvent has a higher temperature than the growing crystal. The solvent used for grow run is supersaturated and growth takes place on self-nucleated seeds in the supersaturated solution because of the temperature gradient difference. Solvents can be transported with both natural and forced convection.

Crystal growth can be carried out either on top of the solution or bottom of the crucible in regard to the temperature gradient direction. Crystal growth on top of the solution with temperature gradient method named the Top-Seeded Solution Growth (TSSG). This method consists of a vertical muffle furnace. The furnace in

Fig.1 is heated by a copper resistance heater and a platinum crucible inside of the heater. Bricks are used to provide heat insulation on both insides of the crucible and the outside of the heater. A seed rotating system is provided on the apparatus.

As an alternative, the seed can be the interior of the solution rather than the top layer. This growth technique is called the dipping solution technique. The high-temperature gradient in the lower part of the solution might be a purpose to use that method for higher growth yield of crystal [1].

In the Fig 2.5 below, an example of a TSSG furnace can be seen. It is a cross-sectional view of the furnace, and all parts are numbered. The crucible is placed in the middle of the furnace and the seed crystal is dipped to the melted from upper section. All other parts are related to heating those are heating elements and heat shields. Also, there is an observation hole at the top of the furnace which is next to the seed rotator.

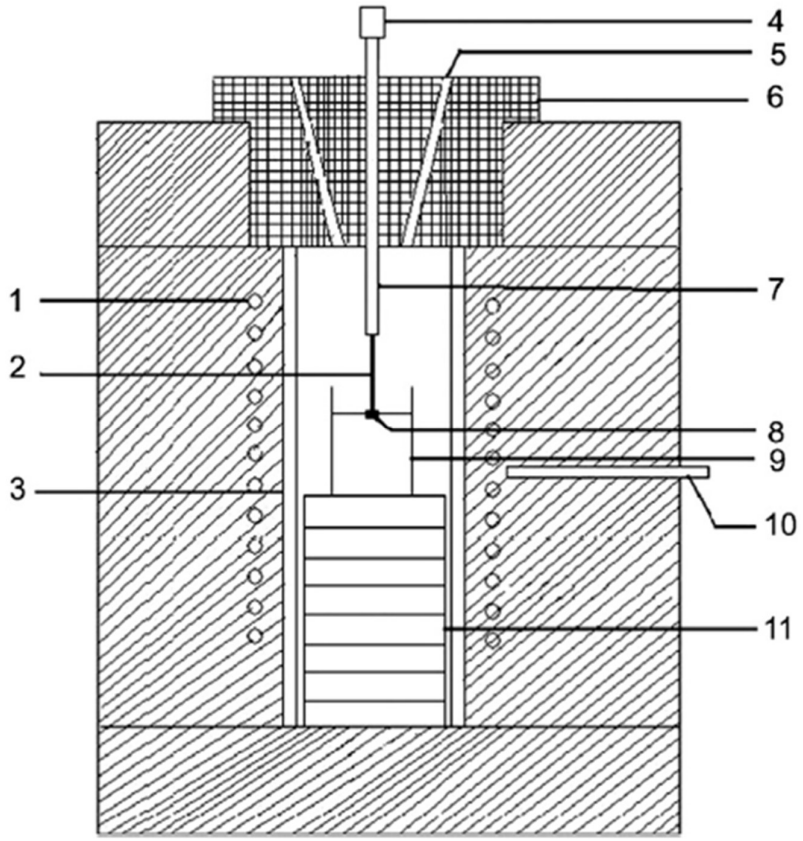

Figure 2.5: Schematic diagram of apparatus used for top-seeded solution growth: (1) resistance heater, (2) platinum rod, (3) alumina tube, (4) seed rotator, (5) observation hole, (6) alumina lid, (7) seed holding rod, (8) mounted seed, (9) platinum crucible, and (10) alumina support [2].

On the Top-Seeded Solution Growth, may develop faceting at the interface that liquid and crystal are coherent. Faceting planes are generally the slowest growing and low-index planes and may lead to deteriorations and lower quality of growing crystal [2]. Also, can trap inclusions of solutions and bubbles, and these cause internal stress. Providing optimal experimental parameters can prevent faceting and it can be satisfied with pre-knowledge and solvent combination.

Crystals can be obtained from different materials and compositions with different muffle and crucible support systems. One technique for using different crucibles is the double crucible system. In the double crucible system, a smaller crucible contains a crystal growth mixture, and a bigger crucible over the smaller one. After the crystal growth is completed, the solution is drained to the bigger crucible and the cooling program starts to cool crucible to the room temperature. However, this study focuses on the single crucible for SiC solution growth.

2.8 Single Crystal Silicon Carbide Growth

It is possible to grow single crystal SiC with the Top Seeded Solution Growth Technique. Starting from the polysilicon charge in the graphite crucible, the furnace is heated above the liquidus line of the system in Fig.2.6 at lower concentrations (1400 °C – 2000 °C). Single crystal material known as seed material is dipped to heated melt. It is used to grow large crystals of the same material. After dipping the seed, it results in the neck formation between the crystal and the melt. At this point, the temperature gradient should be controlled for crystallization. After this point, heat transfer and fluid flow take a place. In the Chapter 3, necessary equations are given for the electromagnetic field, heat transfer, and fluid flow in the melt.

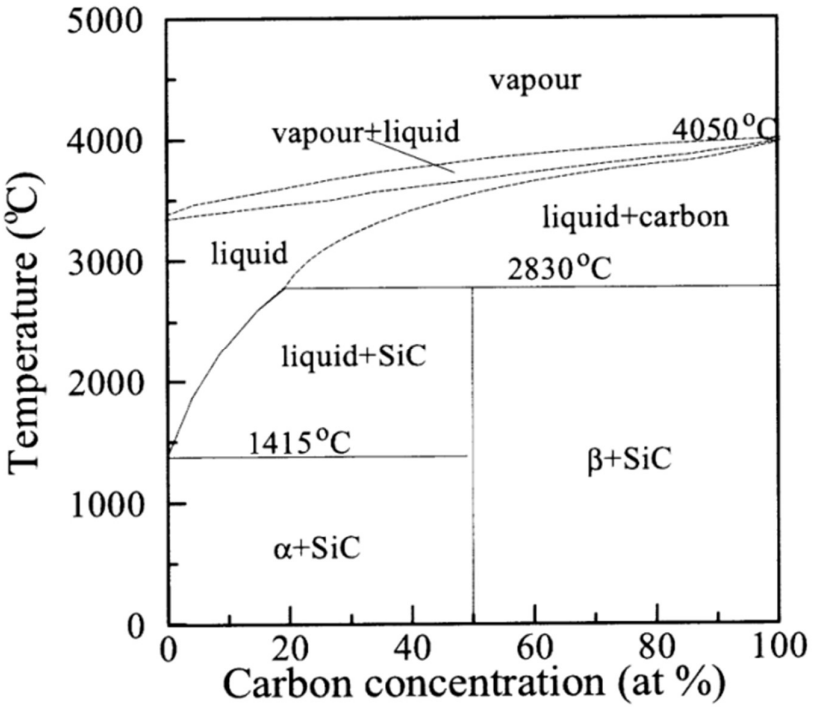

Figure 2.6: Phase diagram of the carbon-silicon system [17].

Chapter 3

Numerical Study

This chapter gives governing equations of the crystal growth system. Those are divided into 3 sections: Electromagnetic Field, Heat Transfer in the Furnace, and Fluid Flow in the Melt. Afterwards, it refers to the modeling of the system (crucible and melting) with given dimensions. For the last part, the assumptions are taken into account and the processes are explained. However, the actual simulation is given in the Chapter 4.

3.1 Electromagnetic Field

For this growth system, the governing equations of the electromagnetic field are obtained from Maxwell's equations. This numerical procedure developed by Gresho and Derby [18]. Also, it is being explained and used by Yamamoto and Dost et al. [19]. They have carried out a three-dimensional numerical study for the Si-C system.

The magnetic field stream function can be introduced as;

$$\Psi(r, z, t) = C(r, z)\cos\omega t + S(r, z)\sin\omega t \qquad (3)$$

$C(r, z)$ is the in-phase component and $S(r, z)$ is the out-phase component of the solution where ω is the frequency and t is the time.

In terms of the in-phase and out-phase amplitudes of the magnetic stream function, the boundary conditions must be specified for this equation;

$$\frac{\partial^2 C}{\partial r^2} + \frac{\partial^2 C}{\partial z^2} - \frac{1}{\mathrm{r}}\frac{\partial C}{\partial r} = \left(\frac{\mu_e \sigma_e \omega}{\mathrm{r}}\right) S \qquad \text{in the conductor} \qquad (3.1)$$

$$= -\mu_e \boldsymbol{J}_0 \qquad \text{in the coil} \qquad (3.2)$$

$$= 0 \qquad \text{in the non-conductor} \qquad (3.3)$$

$$\frac{\partial^2 S}{\partial r^2} + \frac{\partial^2 S}{\partial z^2} - \frac{1}{\mathrm{r}}\frac{\partial S}{\partial r} = \left(\frac{\mu_e \sigma_e \omega}{\mathrm{r}}\right) C \qquad \text{in the conductor} \qquad (3.4)$$

$$= 0 \qquad \text{in the coil} \qquad (3.5)$$

$$= 0 \qquad \text{in the non-conductor} \qquad (3.6)$$

where μ_e is the magnetic permeability, σ_e is electrical conductivity, C is in-phase amplitude of magnetic stream function, S is out-phase amplitude of magnetic stream function, J_0 is peak current in the coil, r is radial coordinate and z is axial coordinate.

Both, Joule heat and Lorentz force densities are time-varying functions with high frequencies [19]. However, they are defined by averaged functions because the time resolution would be impossible for our computational capacities. The period-averaged Joule heat generation and magnetic force densities are given by

$$q = \frac{\omega}{2\pi}\int_0^{\frac{2\pi}{\omega}} \frac{\boldsymbol{J}_\theta}{\sigma_e}\, dt = \frac{\sigma_e \omega^2}{2\mathrm{r}^2}\ (C^2 + S^2) \qquad (3.7)$$

where q is joule heat generation density and where $\boldsymbol{J}_\theta$ is current density. From Eq. 3.1. and Eq 3.2., the related boundary conditions are C=S=0 along boundaries and at the center axis.

$$\boldsymbol{J}_\theta = \boldsymbol{J}_0 \cos \omega t \qquad (3.7.1)$$

$$\mathbf{F}_E = \int_0^{\frac{2\pi}{\omega}} \mathbf{J} \times \mathbf{B} dt \tag{3.8}$$

$$(\mathrm{F}_{E,r}, \mathrm{F}_{E,\theta}, \mathrm{F}_{E,z}) = \left(\frac{\sigma_e \omega}{2r^2}\left(C\frac{\partial S}{\partial r} - S\frac{\partial \mathrm{C}}{\partial r}\right),\ 0,\ \frac{\sigma_e \omega}{2r^2}\left(C\frac{\partial \mathrm{S}}{\partial z} - S\frac{\partial \mathrm{C}}{\partial z}\right)\right) \tag{3.9}$$

3.2 Heat Transfer in the Furnace

$$\nabla \cdot (k\nabla T) + q = 0 \tag{3.10}$$

where T is the temperature, k is the thermal conductivity. In the furnace, heat transfer is assumed to be steady and expressed by Eq. 3.8 energy balance equation. The Joule heat generation density is given by Eq. 3.7. Since the radiative heat transfer is dominant, the effect of thermal convection is neglected.

3.3 Fluid Flow in the Melt

$$\frac{\partial \mathbf{u}}{\partial t} + \mathbf{u} \cdot \nabla \mathbf{u} = -\frac{1}{\rho}\nabla p + \nu \nabla^2 \mathbf{u} + \frac{\mathbf{F}_E}{\rho} \tag{3.11}$$

where t is the time, ρ is the density, $\mathbf{F}_E$ is the Lorentz force density.

This equation is obtained from the momentum balance and the overall mass conversation [19]. The melt is assumed as an incompressible and Newtonian fluid. $\mathbf{F}_E$ is the Lorentz force that has been given in Eq 3.9. Since this is the factor that affects fluid flow directly, simulations are completed to determine Lorentz forces in the Chapter 4. Later, there will be an explanation about which kind of fluid flow is needed in the system and, how it can contribute to the single crystal growth for this process.

3.4 Modeling of the crucible and melt

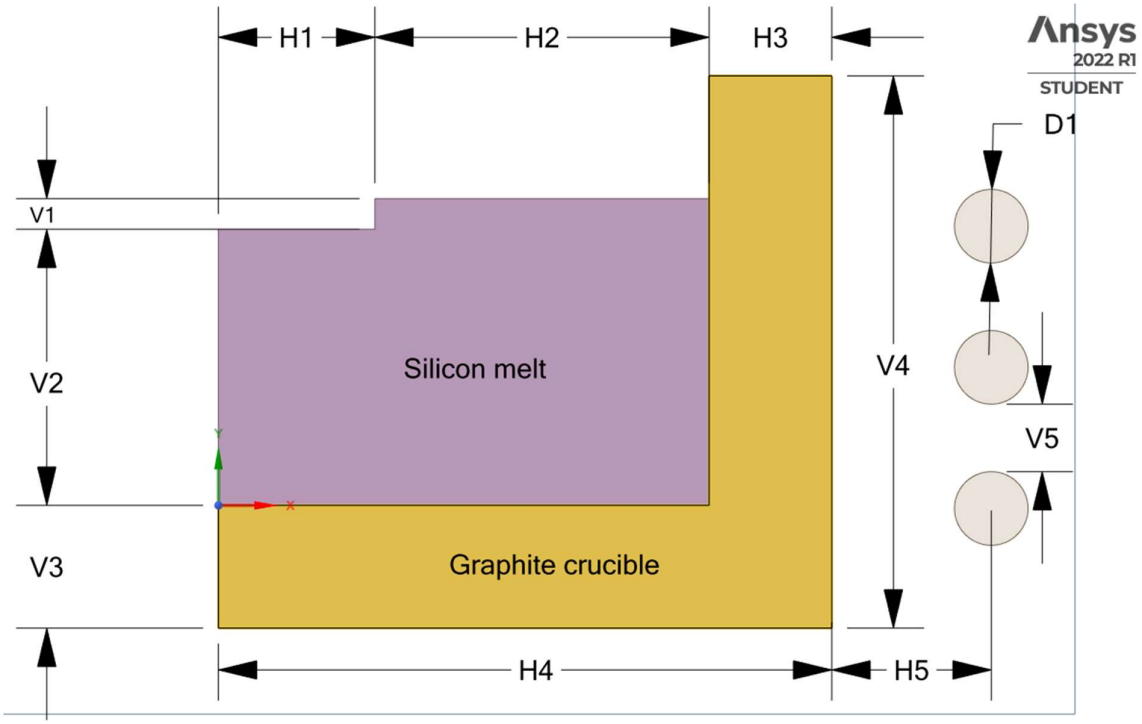

Figure 3.1: 2-D cross-sectional view of the crucible and melt in ANSYS

The cross-sectional view of the numerical domain used in this study is presented in Fig3.1. The graphite crucible is essential for growing SiC crystals. Since there are no carbon atoms in the silicon melt, the only carbon source is the crucible itself. Single crystal seed is not represented here but it is located at the top left part of the silicon melt which is using V1 and H1 dimensions. V1 = 5 mm and H1 = 25.5 mm. When the domain is swept around the Y axis, the seed crystal is on the top center of silicon melt. Respectively, other vertical dimensions are V2 = 45 mm, V3 = 20 mm, V4 = 90mm and V5 = 11 mm. The coil material is selected as copper. Three circles outside of the crucible represent copper coils. The diameter of the circle (D1) is 12 mm and is shared by all copper coils. The distance between copper coils is the same and uses dimension V5. The distance between the coils and the graphite crucible is H5 = 26 mm. Graphite crucible has the length of 100 mm (H4 = 100mm). Other horizontal dimensions are; H2 = 54.5 mm and H3 = 20mm. All parts are being modeled in ANSYS DesignModeler software and all simulations have been done in ANSYS 3-D Maxwell software.

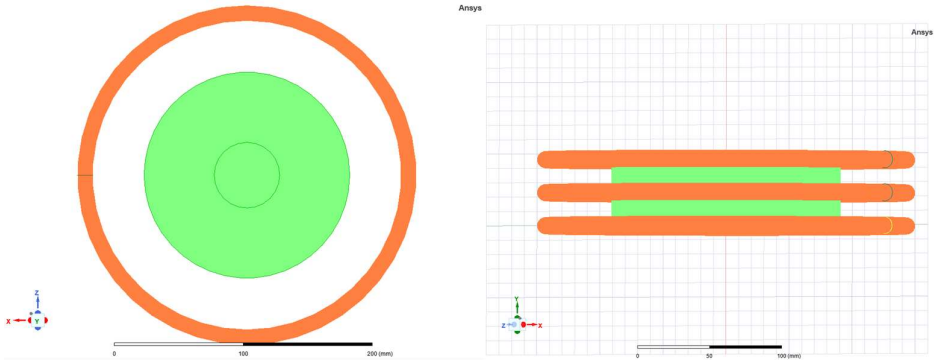

Figure 3.2: Snapshots of three-dimensional numerical domain; top view and side view respectively

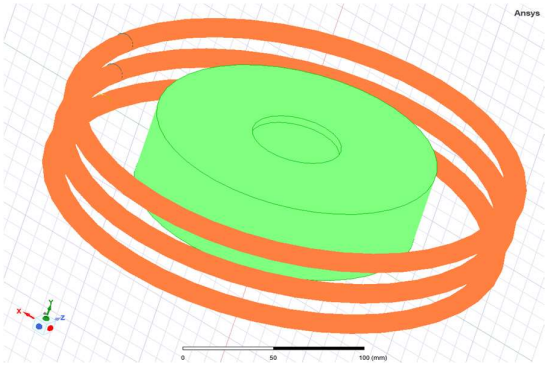

Figure 3.3: Snapshot of three-dimensional numerical domain; isometric view

3.5 Assumptions

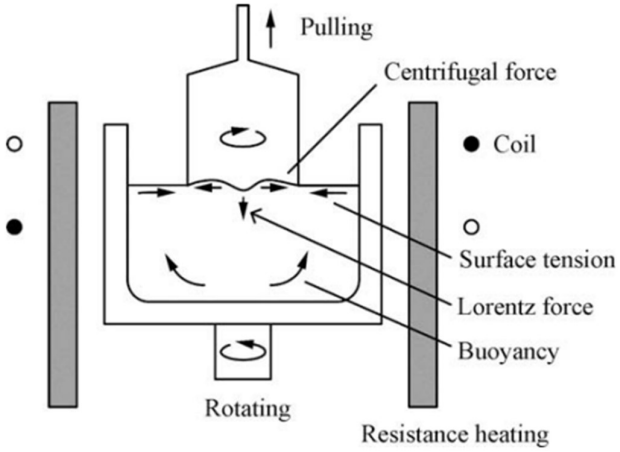

Figure 3.4: Schematic diagram of the melting in the growth process [20].

Since crystal growth are very complex phenomena and the experiments are very expensive and time-consuming, computational numerical simulations has gained importance over years. However, we still need to make assumptions because of our limited computer capacity.

These assumptions are;

1) Electromagnetic field generated by the coil will not contribute to the heating. The furnace was assumed to be heated already by an external heating source (for example resistive heating).
2) In a real-life experiment, as can be seen in Fig3.3, the liquid has surface tension on the free surface (Marangoni effect). This also can affect the driving forces of fluid flow in the melt but the Marangoni effect is neglected for this study. The surface is assumed to be flat.
3) The seed rotation and rotation of the crucible is not taken into consideration. So, the fluid will not have forced convection. This may help to comparison of relative strengths of the Lorentz and buoyancy body forces which is main aim of the study.

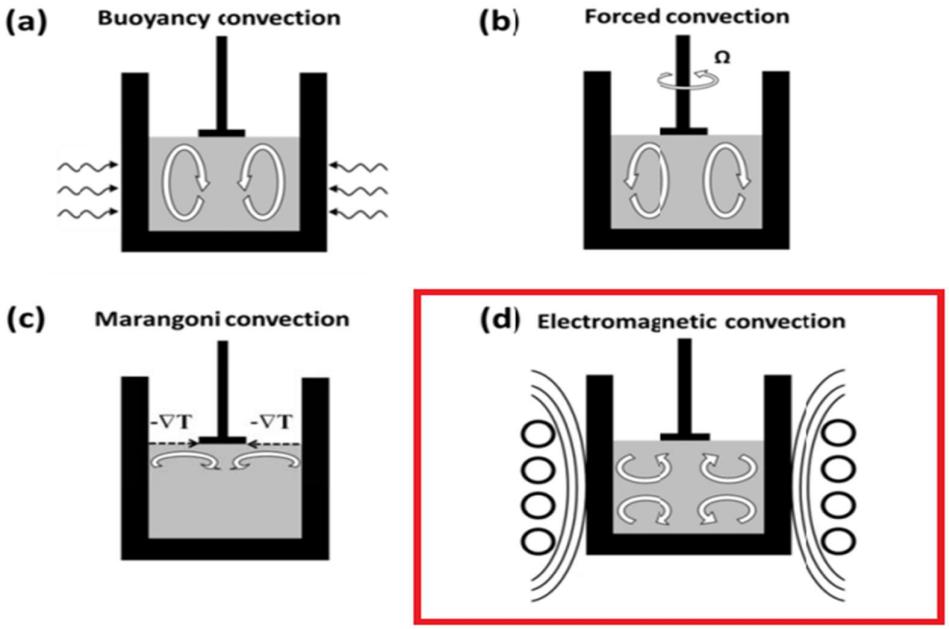

Figure 3.5: The main four convection mechanisms in the fluid [21].

Chapter 4

Simulations

In this chapter, completed simulations of a Silicon-Carbide system are mentioned. This system is considered using a Top-Seeded Solution Growth furnace. The crucible, melting, and induction coils are modeled. These models and dimensions have been given in Chapter 3. All simulations are carried out to determine electromagnetic convection (Lorentz forces) in the system. It focuses change of Lorentz Forces with given frequencies. Later, the comparison against the buoyancy convection is covered. ANSYS Workbench, ANSYS SpaceClaim, and ANSYS Maxwell 3D are software used for the simulations. Setups for simulations had been explained in Appendix A.

4.1 50 kHz Simulation

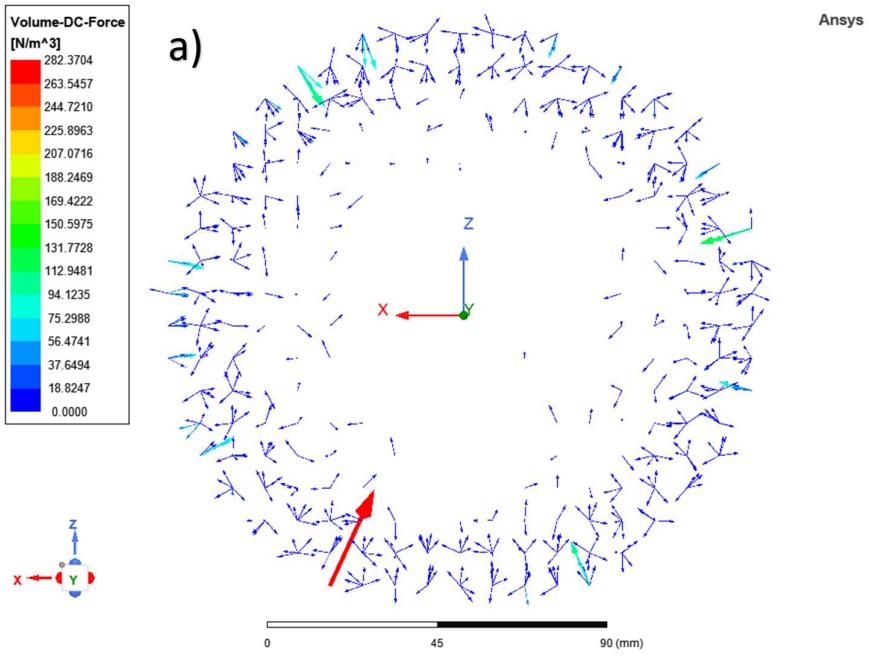

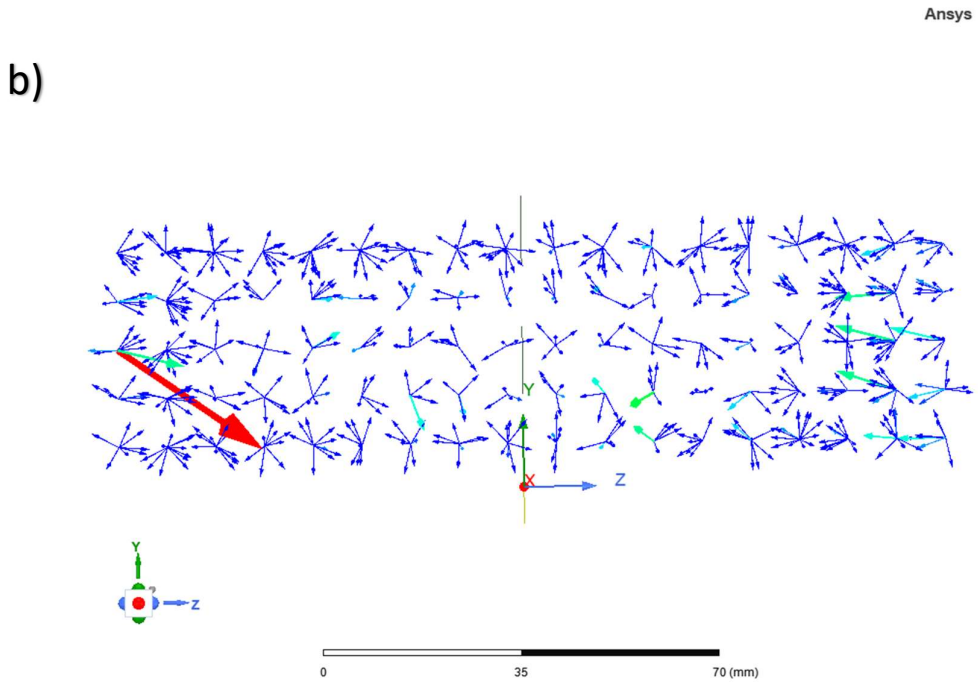

Figure 4.1: Total distribution of electromagnetic forces in the silicon melt for frequency of 50 kHz with the color chart explaining its magnitude; a) top view, b) side view

In Fig. 4.1, the electromagnetic forces(Lorentz forces) can be seen in domains. The complete circle represents the silicon melt. These forces are in the silicon melt which calculates equation 3.8 and equation 3.9. The current density of the coil is selected as 100 Amperes. The working frequency is selected as 50 Kilohertz. These domains indicate its direction and magnitude. Also, there is a color chart which is useful to understand its value. In this case, the maximum force will be approximately 282.37 N/m^3.

This force value is important to control fluid flow in the melt. Since the graphite crucible is the only source of the Carbon atoms and the seed crystal is SiC. Accordingly, SiC growth is the aim of this process. In order to maintain successful growth, carbon atoms should be transported from the crucible wall to the seed in the middle. Although, there will be a temperature difference between the crucible walls and the seed. This will cause buoyancy convection which is schematically represented in the Fig 3.5. Later on, these values will be compared, and it will show if the melt is electromagnetic convection controlled or buoyancy convection controlled. However, as can be seen in the Fig 4.1, there are no domains in the center of silicon melt. This means Lorentz forces do not extend to the center of the melt which means this frequency is not suitable for this process. Also, all domains are randomly distributed, so it will not benefit in any way. Fig 4.2 shows the total

magnetic flux density in the silicon melt with the same current density. This may give an idea about why it does not penetrate the center. In the next chapter, the same simulation is conducted with a new frequency.

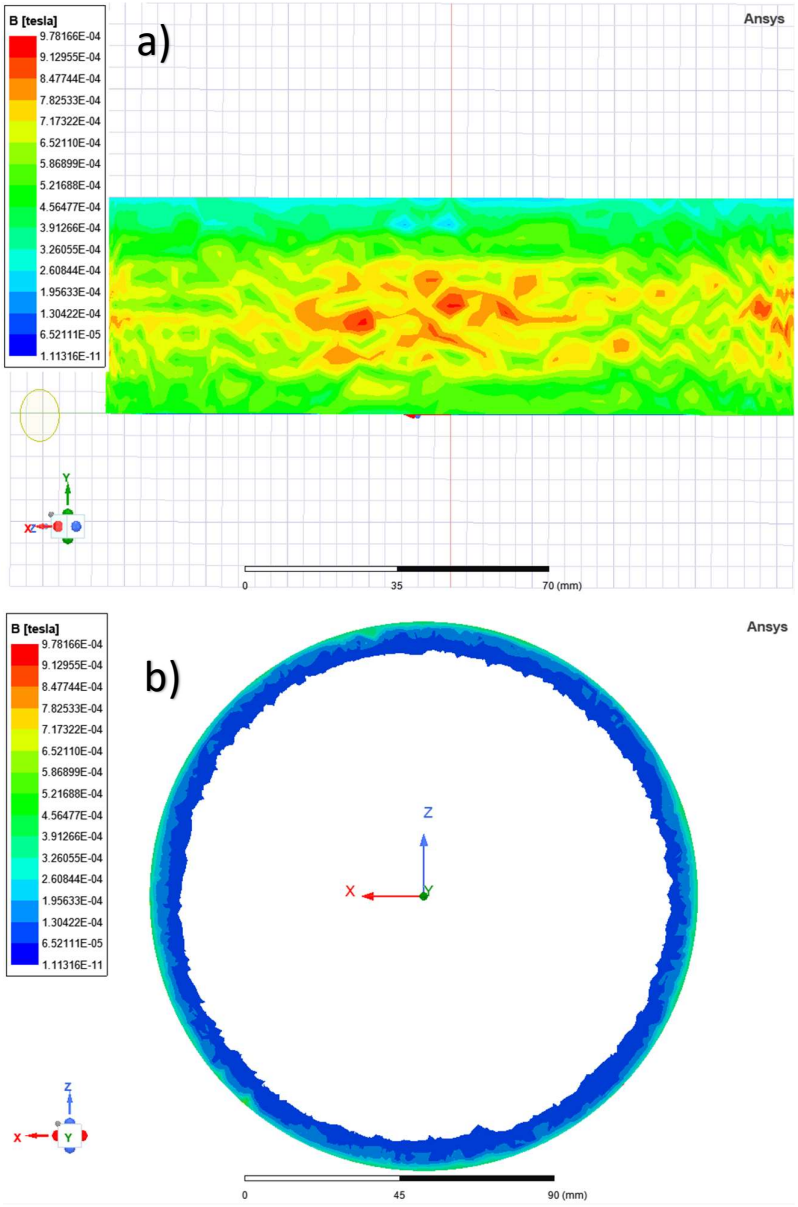

Figure 4.2: Total magnetic flux density in the silicon melt for frequency of 50 kHz with the color chart explaining its intensity ; a) side view, b) top view

4.2 50 Hz Simulation

For this simulation, all parameters are the same as the Section 4.1. However, the frequency was 100 times greater in the first simulation. 50 Hz is the selected frequency for this simulation. The results can be seen in the Fig 4.3 below.

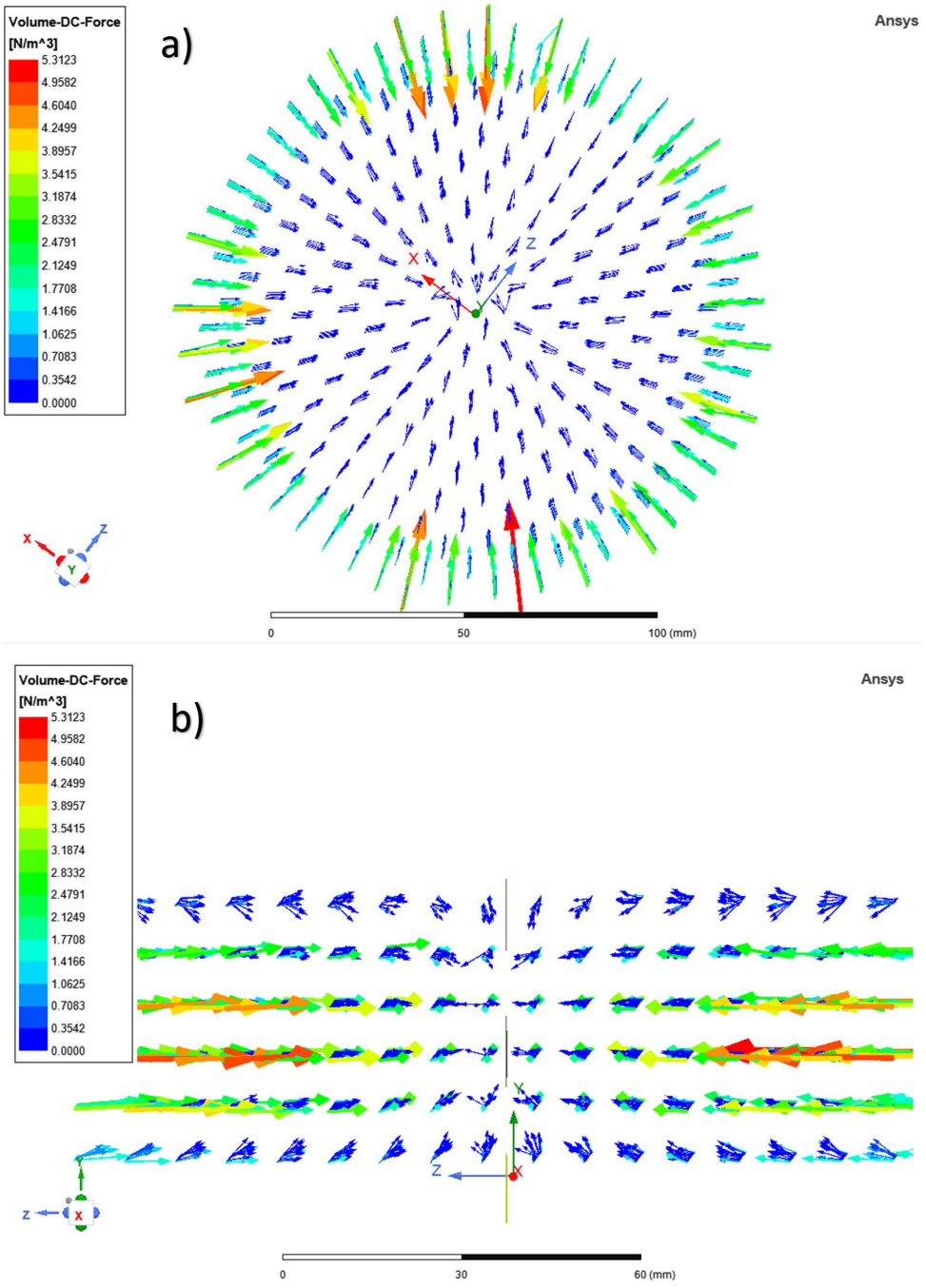

Figure 4.3: Total distribution of electromagnetic forces in the silicon melt for frequency of 50 Hz with the color chart explaining its magnitude; a) top view, b) side view

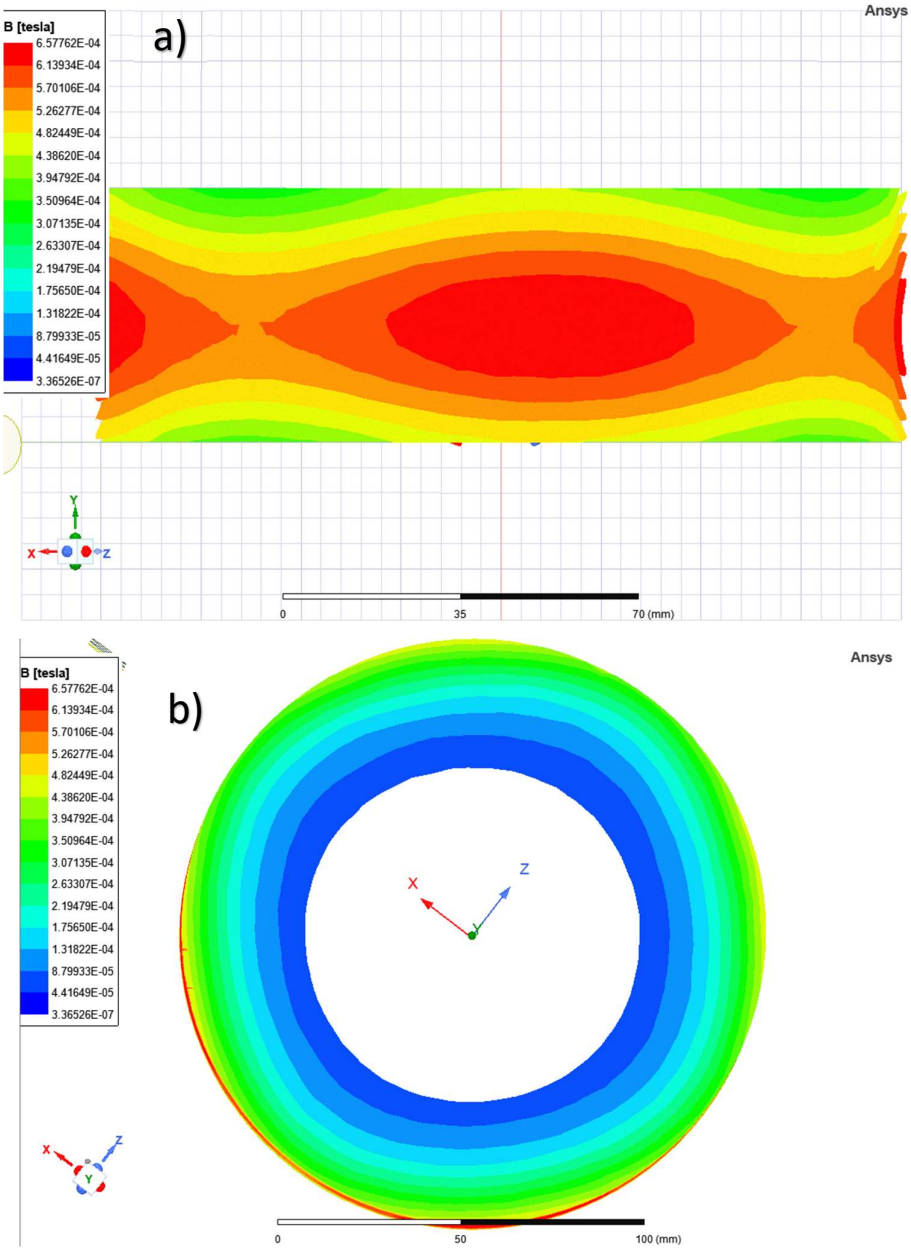

Figure 4.4: Total magnetic flux density in the silicon melt for frequency of 50 Hz with the colors chart explaining its intensity; a) side view, b) top view

Domains are perfectly aligned through the center. There are many domains in the middle of melt and, the forces are coming from all sides equally. It does reach the SiC seed without a discontinuity. This kind of fluid flow is absolutely wanted for this kind of application. However, the problem with this frequency is, generated forces are significantly less. The maximum force is calculated as 5.31 N/m^3. This

low amount of force will not be enough to suppress buoyancy forces. Because of this, an adequate frequency should be used. In order to find that frequency, the simulation is repeated many times with different frequencies.

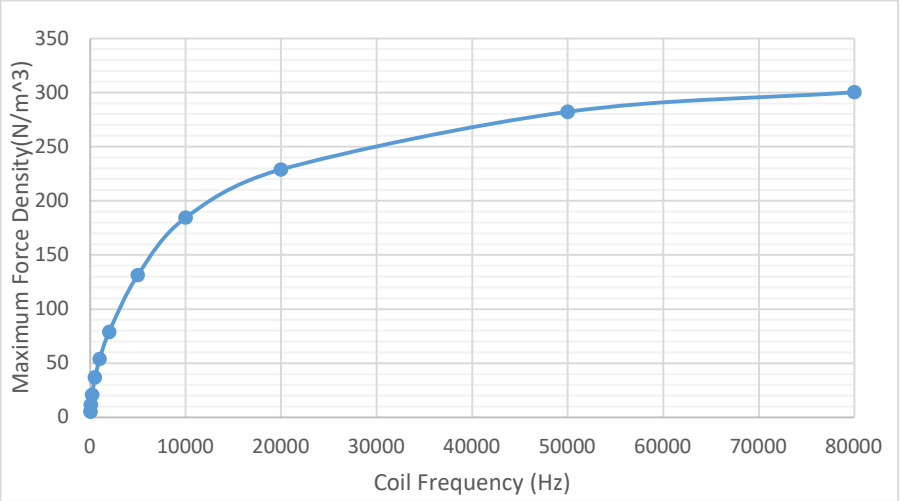

Figure 4.5: Coil frequency (range of 0-80000 Hz) as a function of maximum generated force density in the silicon melt.

In the Fig 4.5, all dots are indicating calculated the maximum force density with different frequency simulations. Even though higher frequencies have greater force densities, those are not penetrating to the middle, basically, it does not reach the seed which is an insufficient condition for growth.

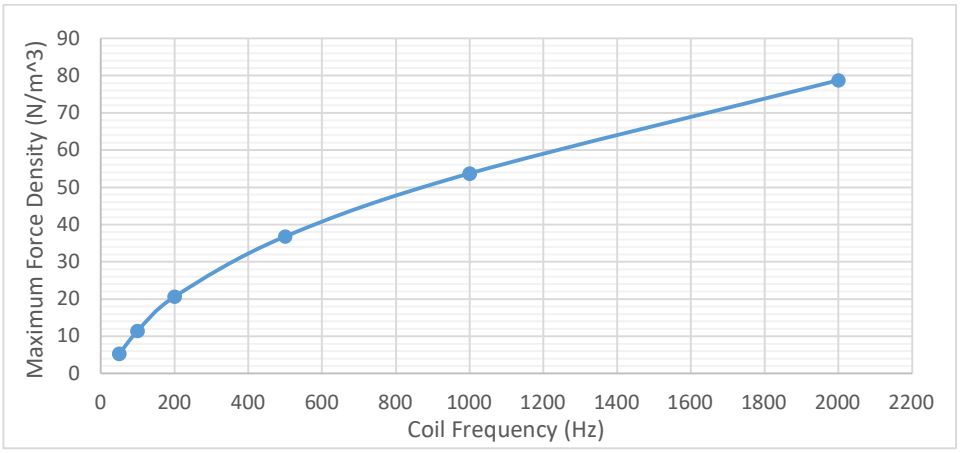

Figure 4.6: Coil frequency (range of 0-2000 Hz) and maximum generated force density in the silicon melt.

The frequency range in Fig 4.6 may have better results in terms of force and penetration balance. To calculate this exactly, buoyancy forces should be calculated. In the next section, the necessary equation and calculations will be given for the silicon melt. Afterwards, it can be compared to the forces from simulation results.

4.3 Buoyancy Forces in the Silicon Melt

As mentioned in chapter 3, the silicon melt has many forces for driving fluid flow. Since there is a free surface, one of these forces is a free surface gradient (Marangoni effect). However, it is neglected in this study. Also, this system assumed stationary which makes cancels forced convection out. The remaining forces are Buoyancy body forces and electromagnetic (Lorentz) body forces. The simulations are completed to determine electromagnetic forces and buoyancy body forces are calculated by hand in this section.

Due to the temperature difference in the system, buoyancy forces appear in the silicon melt. Thus, for calculating buoyancy body forces, the Boussinesq approximation must be taken into account when working with incompressible fluid models. The formula for calculating buoyancy body force [22] is;

$$\boldsymbol{F}_{Buo} = \alpha g \rho (T - T_{ref}) \tag{4.1}$$

where $\boldsymbol{F}_{Buo}$ is the buoyancy body force, $\boldsymbol{\alpha}$ is the thermal expansion coefficient of the pure silicon, $\mathbf{g}$ is the acceleration($9.81\ m/s^2$), $\boldsymbol{\rho}$ is the density. For this case $\mathbf{T}$ is temperature in Kelvin.

$$\alpha = 1.4 \times 10^{-4}\ K^{-1}$$

$$\rho = 2550\ kg\ m^{-3}$$

$$\mathbf{F}_B = 2550 \times 9.8 \times 1.4 \times 10^{-4}(T - T_0) = 3.499(T - T_0) \tag{4.2}$$

This equation equals $3.499(T - T_{ref})$ which is directly related to the temperature difference. After putting the temperature, Kelvins will cancel out and

its unit will be Newton. For example, if the temperature difference is 20° K in the system, this will make approximately 70 Newton buoyancy body force. In the Fig 4.8 below, the relation between temperature difference and buoyancy body forces can be seen.

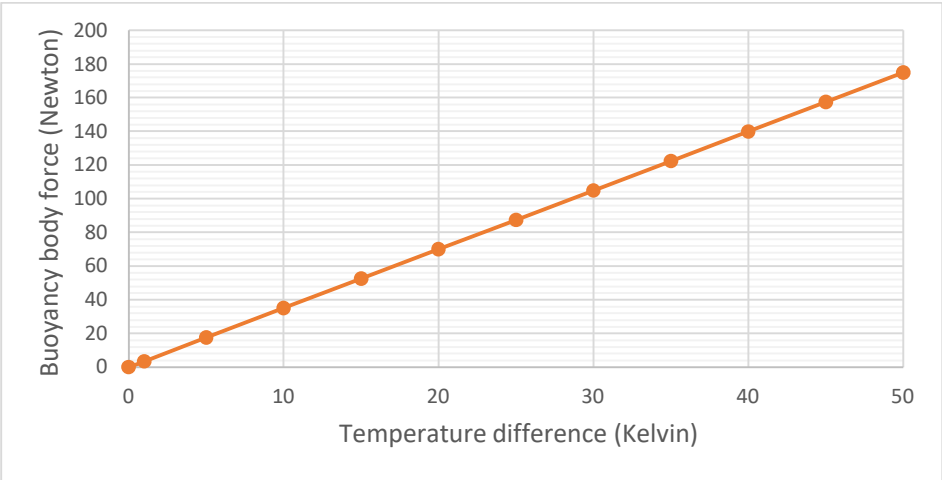

Figure 4.7: Temperature difference – buoyancy body force relation which is calculated from buoyancy body force formula

According to this calculation, the temperature difference range of 0 - 50° K generates buoyancy body forces that range from 0 - 174.95 N. In order to compare buoyancy body forces with electromagnetic forces, Fig 4.7 is analyzed. Respectively, the simulation with 1 kHz frequency has a maximum of 53.71 N force as a result and, the simulation with 500 Hz frequency has a total of a maximum of 36.80 N force.

4.4 800 Hz Simulation

For this simulation, 800 Hz frequency generates a maximum of 47.53 N force total. If we take this force and compare it with the buoyancy forces, it can be used for a 15° K temperature difference in the system. The fluid flow in the melting will be electromagnetic convection controlled rather than buoyancy forces if the temperature difference is lower than 15 ° K.

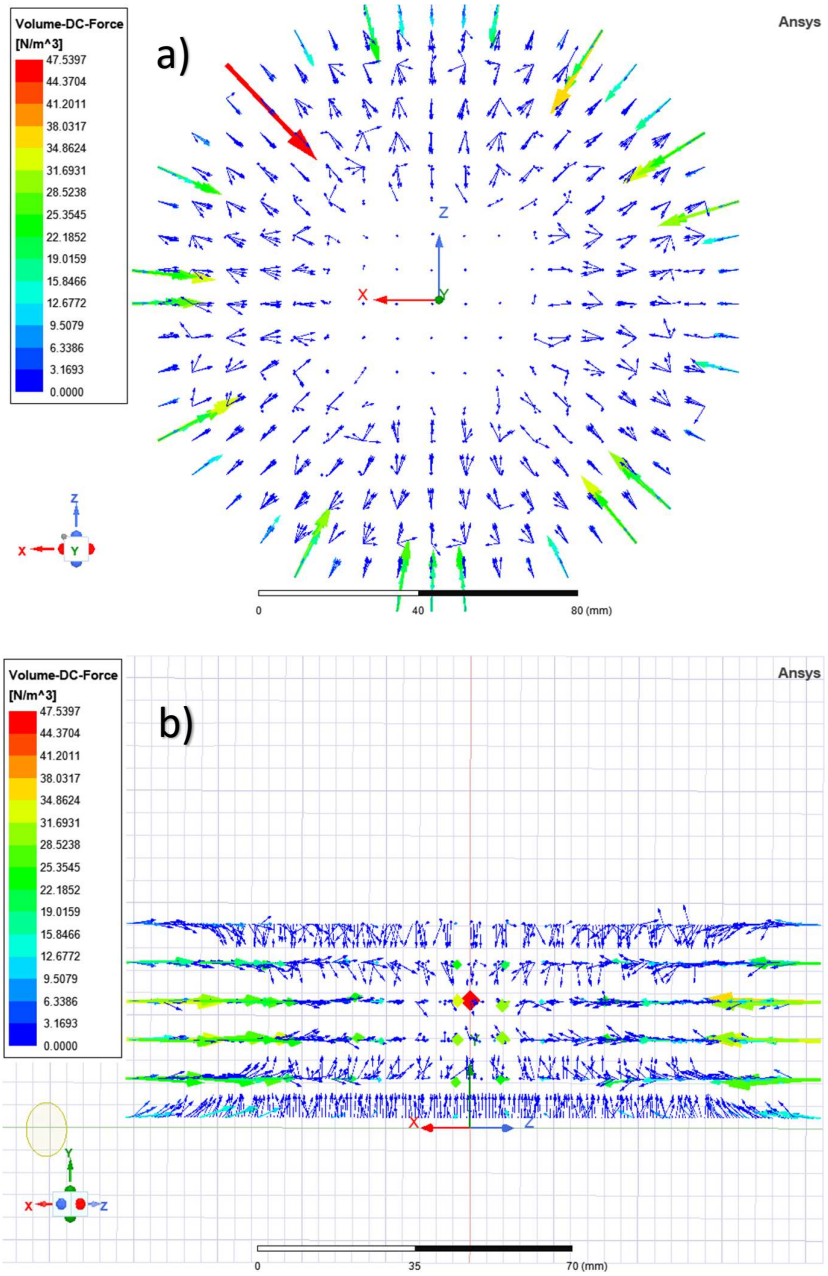

Figure 4.8: Total distribution of electromagnetic forces in the silicon melt for frequency of 800 Hz with the color chart explaining its magnitude; a) top view, b) side view

The alignment of domains is looking promising for this frequency and most domains are extended to the boundaries of the seed. Their direction is correct which means most of them are coming from the hot crucible walls to the cold seed. As mentioned early, this is needed for the transportation of Carbon atoms. Since this is a 3-D model, isometric views may help to see it better.

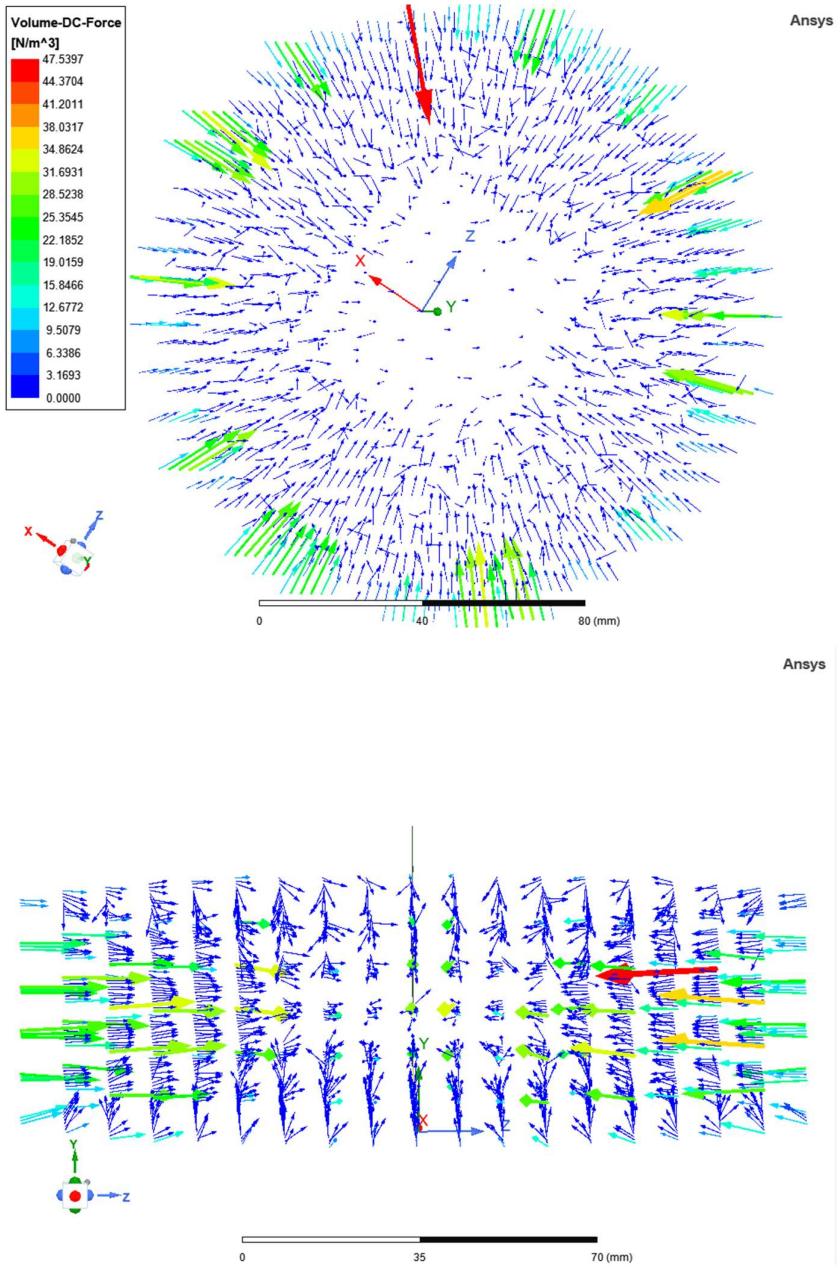

Figure 4.9: Total distribution of electromagnetic forces in the silicon melt for frequency of 800 Hz with the color chart explaining its magnitude; isometric views

As can be seen in Fig 4.10, this frequency is close to the solution, but it does not guarantee that carbon atoms can reach the center since there are no aligned domains in the seed area. This may be caused by the large crucible diameter which is mentioned in the Section 3.4 as the modeling of the crucible. This experiment needs to be repeated with adjusted crucible dimensions. However, changing this will change the furnace design also. Because coils must be adjusted according to

the crucible. This change will be mentioned in Chapter 5, Discussion. Before that, the simulation with 500 Hz frequency should be mentioned and, the simulation results with an adjusted crucible should be mentioned in this chapter. Since buoyancy body forces are already calculated for different temperature gradients in the last section, the electromagnetic forces should be compared for all simulations starting from this chapter.

4.5 500 Hz Simulation

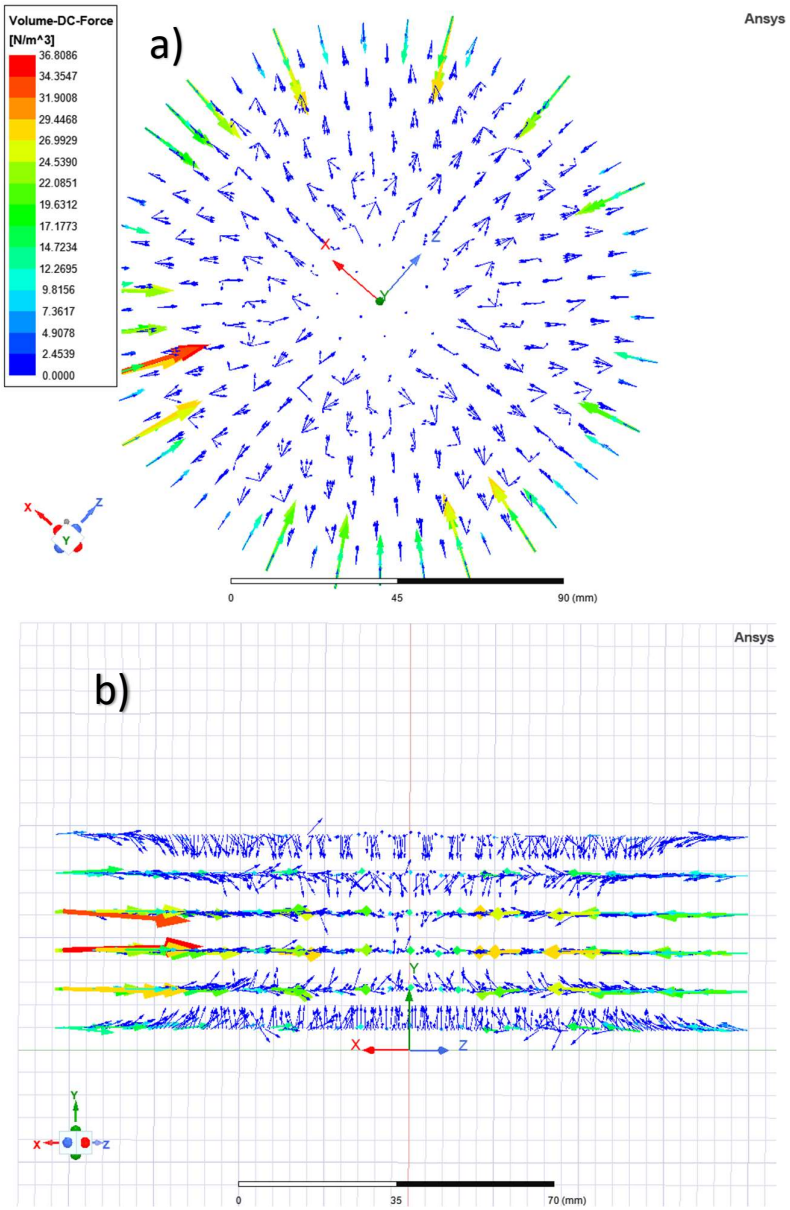

Figure 4.10: Total distribution of electromagnetic forces in the silicon melt for frequency of 500 Hz with the colors explaining its magniude; a) top view, b) side view

The maximum electromagnetic force density is 36.80 N in this simulation which equals to 10.5° K temperature difference for the system or less. This means electromagnetic forces will surpass buoyancy body forces and, will be controlled by electromagnetic convection if the system has a maximum 10.5° K temperature difference. Most domains are directly aligned to the center and there are some domains in the middle of the melt(seed area). It is slightly better than the 800 Hz simulation in terms of fluid flow direction and domain number. However, in order to surpass buoyancy forces, it can have a maximum 10.5° K temperature difference which is 5° K less than the 800 Hz simulation.

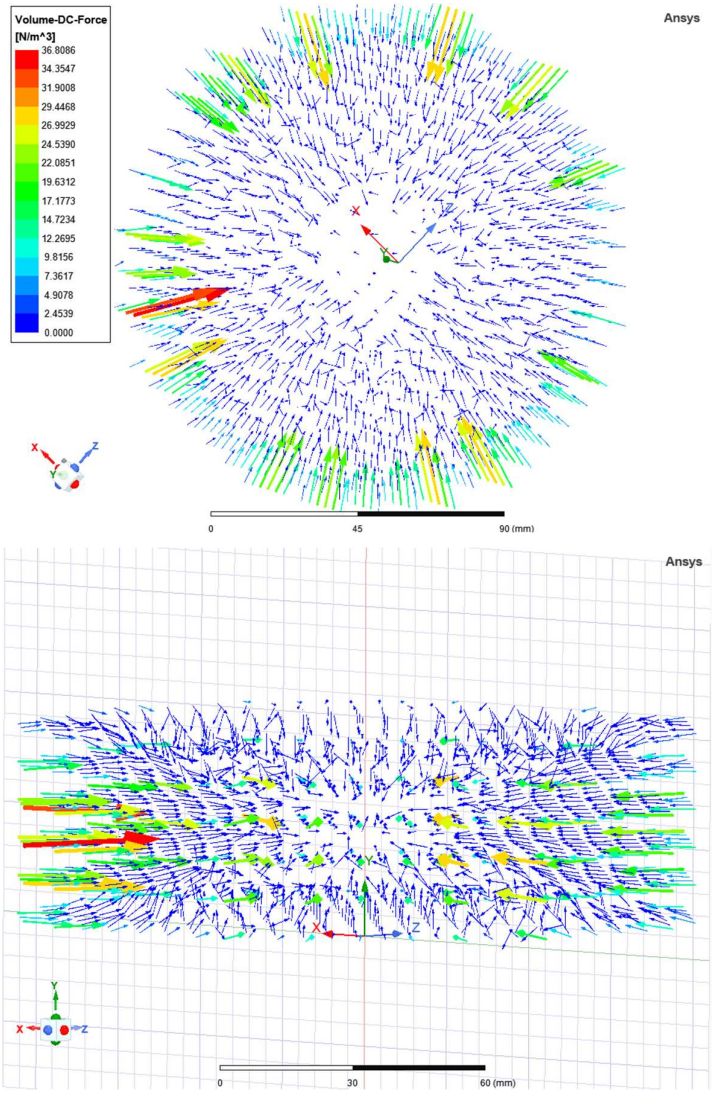

Figure 4.11: Total distribution of electromagnetic forces in the silicon melt for frequency of 500 Hz with the colors chart explaining its magnitude; isometric views

4.6 800 Hz Simulation with Adjusted Crucible Size

For this simulation, all other parameters and dimensions were kept the same as the others except the crucible diameter. The original diameter was explained in the Section 3.4 which was H4 = 100mm. This is reduced by %25 which equals 25 mm. Respectively, coils should be 25 mm closer which changes the furnace design. This may provide better penetration of the electromagnetic forces through the center, and it may generate more forces in the melt.

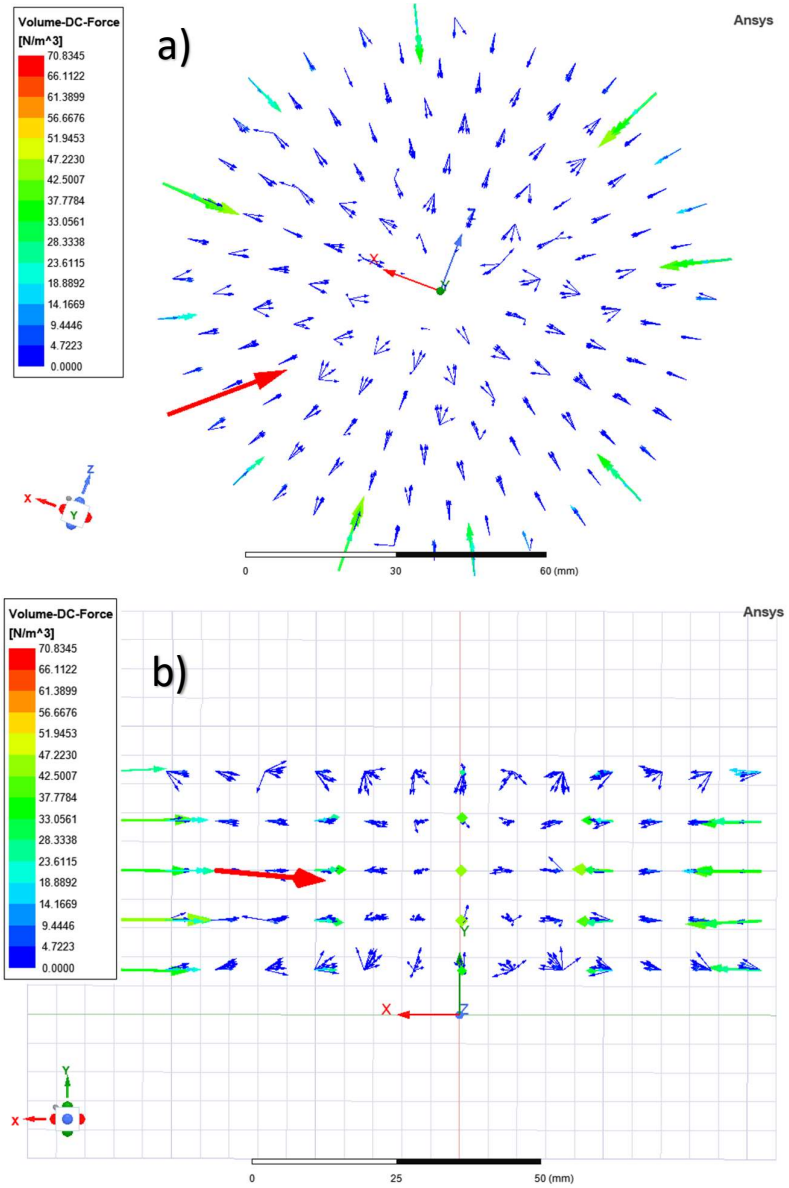

Figure 4.12: Total distribution of electromagnetic forces in the silicon melt for frequency of 800 Hz (adjusted crucible) wit the color chart explaining its magnitude; a) top view, b) side view

As can be seen in Fig 4.12, using a smaller crucible has improved generated total electromagnetic force from 47.53 N to 70.83 N. Also, there are better domains in the silicon melt and forces are reaching the seed. This can be considered a good improvement. Thus, this force will allow using a maximum 20° K temperature difference in the system against buoyancy forces. It also allows using a 5° K higher temperature difference compared to the result from regular-sized crucible simulation. Isometric views in Fig 4.13 below shows that all domains faced towards to the center(seed area) which are expected to contribute growth. Even though smaller crucible will result in smaller diameter of grown crystal, it may have better uniformity because electromagnetic forces are coming from all sides similarly. This should be result in better carbon transportation from the crucible walls to the seed. Amongst all simulations, using 800 Hz frequency and using adjusted(25 mm smaller) crucible has best results overall in terms of electromagnetic force distribution and its magnitude. Higher frequencies are providing very bad electromagnetic force penetration and lower frequencies are providing less generated force in the system. Because of that, 800 Hz can be considered as a good spot for this kind of application for balancing both parameters.

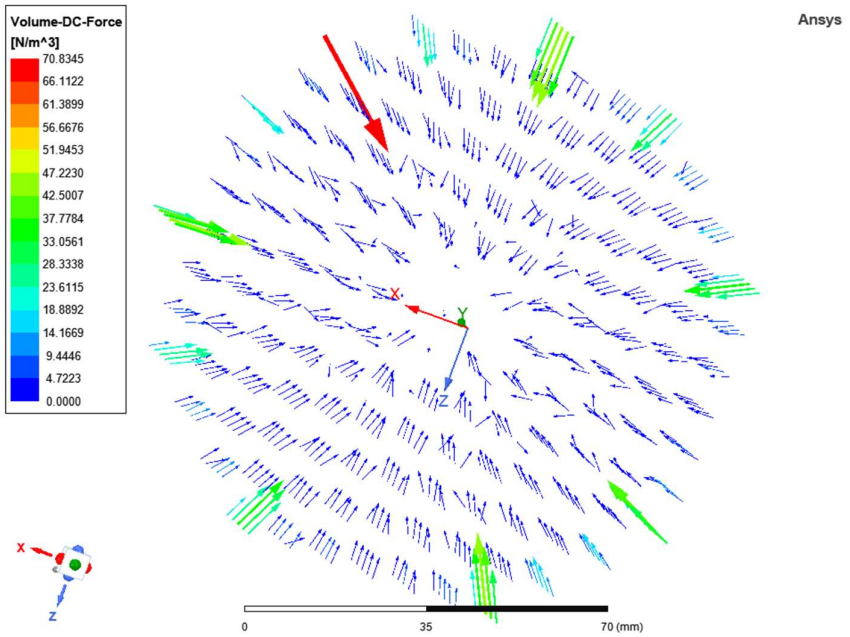

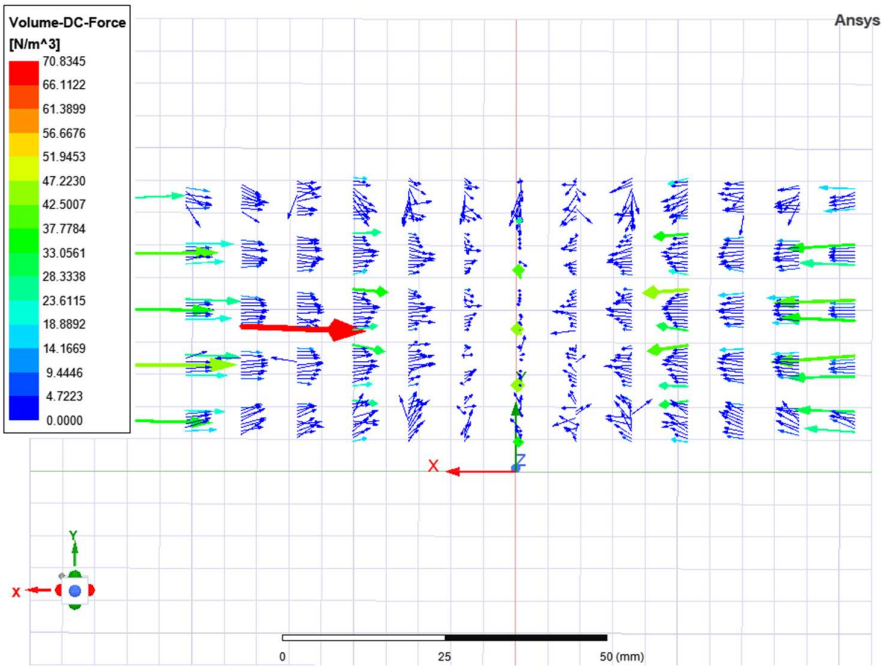

Figure 4.13: Total distribution of electromagnetic forces in the silicon melt for frequency of 800 Hz (adjusted crucible) with the color chart explaining its magnitude; isometric views

4.7 Optimization of Crucible Size

In the last section, the effects of changing crucible size on electromagnetic convection are analyzed. According to the simulation results, the working frequency has been optimized for this kind of process. Also, it can be seen that reducing the crucible size is another variable for better electromagnetic convection. For this purpose, crucible size change is analyzed in this chapter. The simulation is repeated many times with changing crucible diameter (H4) which is explained in section 3.4.

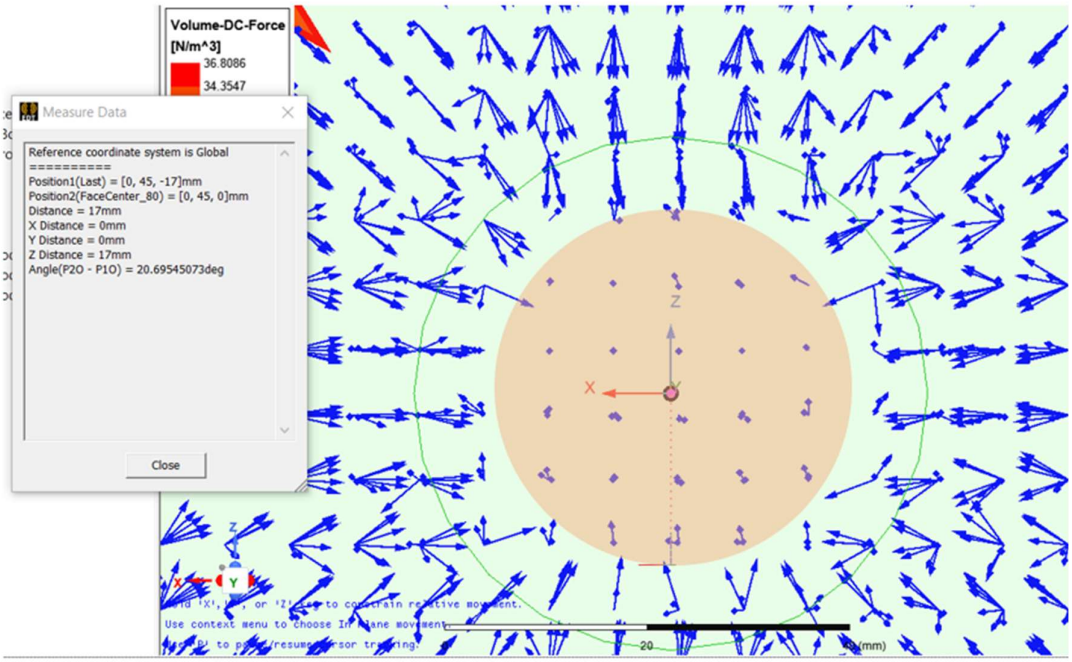

Figure 4.14: Total distribution of electromagnetic forces in the silicon melt for frequency of 500 Hz with original H4 diameter; zoomed in

In Fig 4.14, the electromagnetic forces in silicon melt can be seen clearly. The outer green circle represents the silicon seed which is dipped into the melt. The radius of the silicon seed and other dimensions are given in chapter 3.4. As mentioned earlier, all electromagnetic force domains do not reach the center of the original crucible size. There is an orange circle that touches the last effective electromagnetic force domain. This means electromagnetic force domains inside the orange circle are so small that negligible. Because of this, the crucible small gets smaller in each simulation to the point where all electromagnetic forces reach the center. The aim of this process is to find the optimal crucible diameter that works for a certain frequency. Later on, this optimal crucible diameter will be mentioned as the maximum crucible size that can be used. The radius of the orange circle is 17 mm for the original crucible size. In other words, effective electromagnetic forces are 17 mm far away than the center point of the silicon seed.

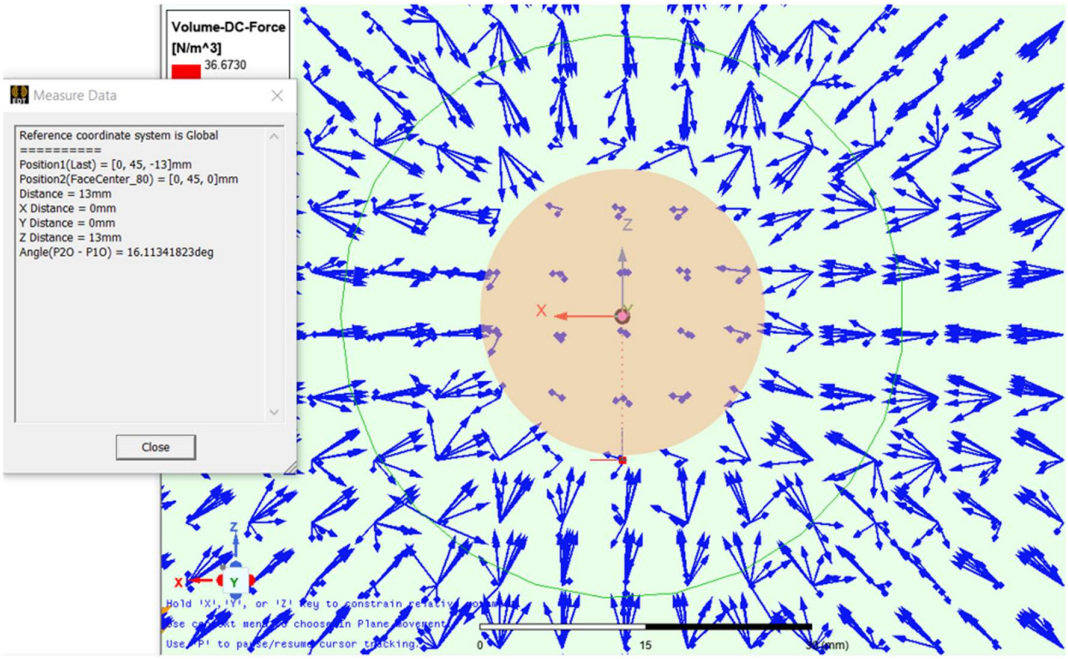

Figure 4.15: Total distribution of electromagnetic forces in the silicon melt for frequency of 500 Hz with 5 mm smaller crucible; zoomed in

In Fig 4.15, it is shown that reducing the crucible size by 5 mm reduced the radius of the orange circle by 4 mm. Original diameter of the crucible (H4) was 100 mm. In this simulation, the diameter of the crucible is 95 mm. By repeating these simulations, the graph below is given.

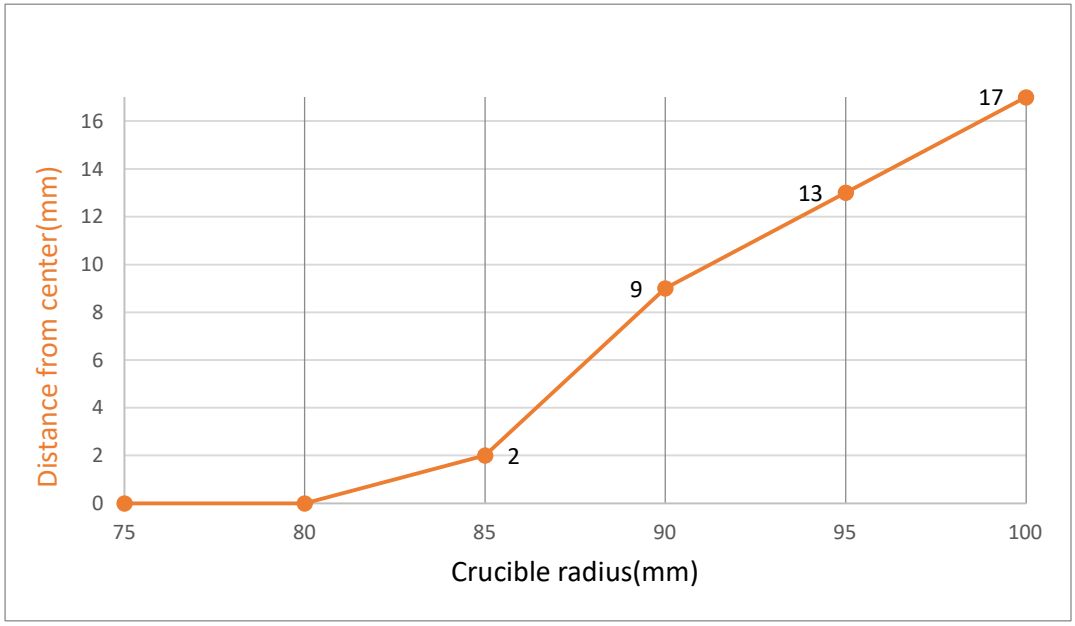

Figure 4.16: Distance of electromagnetic forces from center – Crucible size relation

In Fig 4.16, it can be seen that reducing the crucible size by %10 has the distance of 9 mm from the center which still contains a big gap.

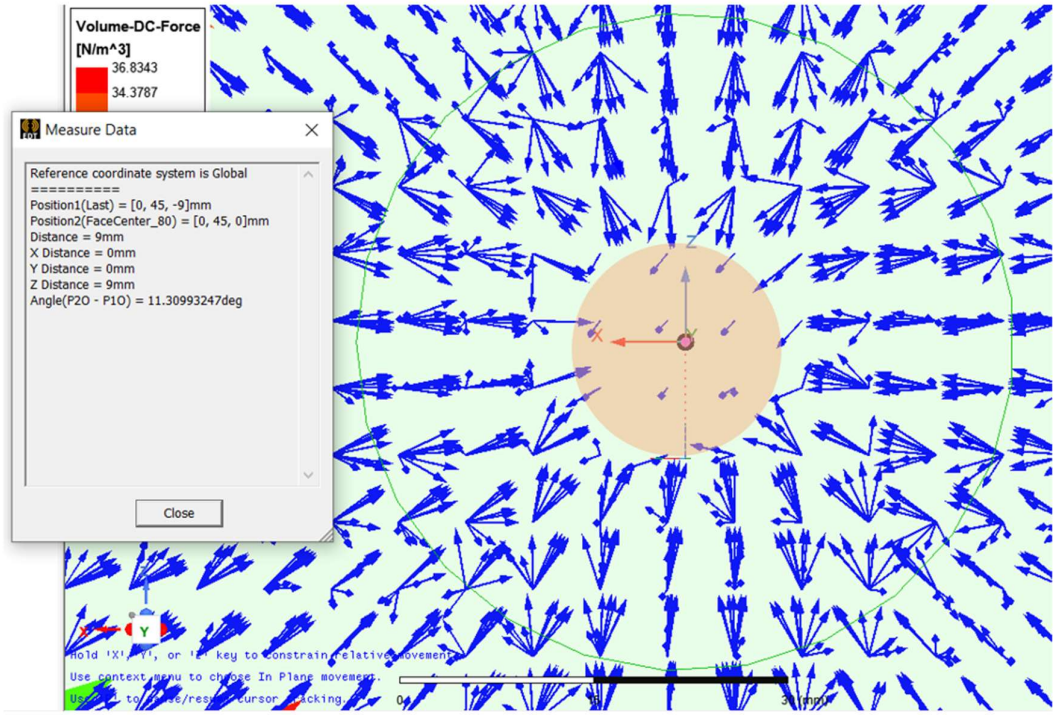

Figure 4.17: Total distribution of electromagnetic forces in the silicon melt for frequency of 500 Hz with 10 mm smaller crucible; zoomed in

The crucible size of 85 mm has better electromagnetic penetration than 90 mm as expected. It is only 2 mm far away from the center. Since this is so small, it can be selected as the maximum crucible size for this process. Another important factor is the change of maximum generated force with crucible size. However, this does not cause any problems since the changes are too small. In Fig 4.18 below, there is a similar graph to Fig 4.17 but with maximum generated forces included. Also, it shows crucible size change instead of maximum crucible size.

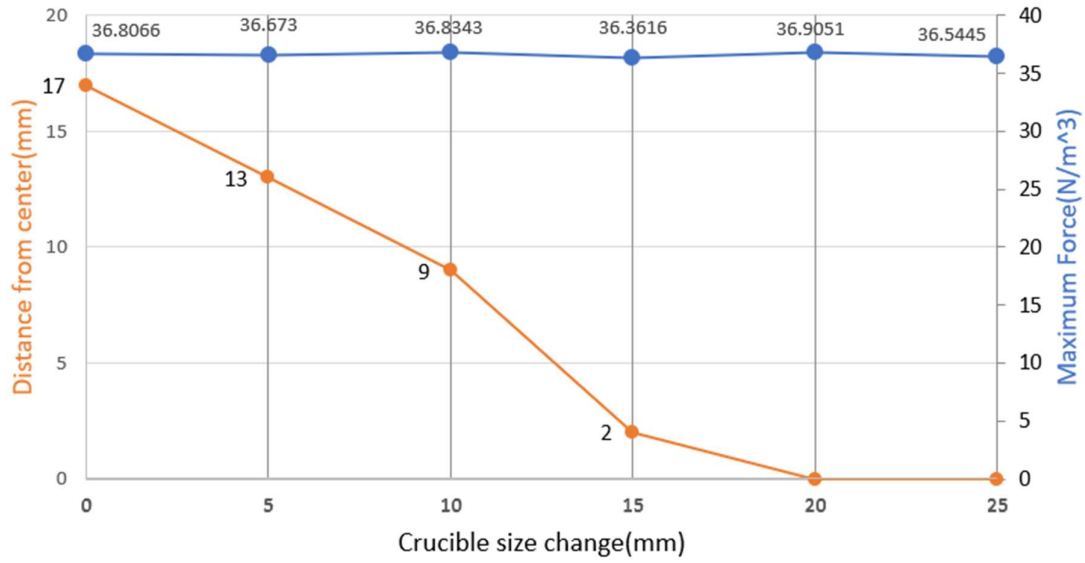

Figure 4.18: Distance of electromagnetic forces from center – Change in crucible size – Maximum generated electromagnetic force relation

Fig 4.18 shows the distance of electromagnetic forces from the center in orange color which is on the left axis. The bottom axis is a change in crucible size which is shared by both the left and right axes. The right axis is the maximum generated electromagnetic force which is colored blue. Also, the value for each point can be seen in the graph. It is obvious that the change in maximum generated electromagnetic force is very small and only changes the fraction. All results from this section are discussed in chapter 5 section 3.

Chapter 5

Discussion

In this chapter, the simulation results from Chapter 4 are discussed in 2 parts. Those parts include electromagnetic force distribution with varying frequencies and effects of the adjusted crucible size in the system. Since the comparison with buoyancy forces and electromagnetic forces is given in Chapter 4, this chapter are explaining the outcome which is the research objective of this study. Finally, this chapter ends with the future work section where assumptions are discussed. This is related to what can be done in future for this topic and it explains how better simulations can obtained.

5.1 Effects of the Frequency Change

In Chapter 4, simulations are tested for many frequencies in the coils between 50 Hz – 50 kHz range. The necessary graphs are given in the Fig 4.5 in Section 4.2. Using higher frequencies in the coils are resulting higher electromagnetic force density in the silicon melt. Despite of this, there are no meaningful force domains in the system after a frequency of 800 Hz. This means force domains do not reach the center where the seed crystal is. Even though there are many force domains near crucible walls, those can not contribute to single crystal growth. Also, most of their directions are random which is another thing that can contribute negatively to the growth.

On the contrary, using low frequencies in the coils has better force distribution and the most force reaching the center. However, lower frequencies have generated lower electromagnetic force density in the system. This may cause fluid flow controlled by buoyancy forces which are not wanted for this application. Frequencies between 500 Hz – 800 Hz have provided adequate electromagnetic force density with good penetrating. Some force domains are reaching the seed crystal. According to the buoyancy force density calculation, generated force from 800 Hz frequency will make the fluid flow electromagnetic convection controlled if the temperature difference in the system is equal to or less than 15 $^{\circ}$ K. As mentioned earlier, not all domains reach the center for this frequency and therefore this solution should be extended. In the next chapter, crucible size is discussed in order to solve this problem.

5.2 Adjusted Crucible Size

The outcome of the simulation has shown the relation between electromagnetic forces and coil frequencies. Nevertheless, the solution needs to be extended in order to control fluid flow completely. This only can be done with full penetration of the electromagnetic through to the center of the silicon melt. The crucible size is an important factor in this issue. All simulations were repeated with adjusted crucible size (reducing the crucible size by 25%). Adjusting the crucible is explained in the Section 4.6 which refers to the model of the crucible. The length of the crucible was 100 mm, and it is changed to 75 mm. The original crucible model with dimensions can be seen in the Section 3.4. This change has provided a significant positive effect on electromagnetic forces distribution and quantity. In the system, generated electromagnetic forces have improved by 50%. This improvement may allow using higher temperature differences in the system as mentioned in the Section 4.6. Moreover, almost all force domains are reached to the crystal for 800 Hz frequency simulation which may provide better fluid flow control against buoyancy forces.

On the other hand, using a smaller crucible size may cause a small diameter of the grown crystal if the crucible size is too small. For this kind of application, mostly bigger crystals are desired. Because of that, this may be counted as a negative side effect of the adjusted crucible size. In this study, the diameter of the seed crystal was the same for all simulations. Furthermore, the furnace design should be changed for using a smaller crucible since the crucible size is dependent on the furnace. Using a smaller crucible without changing the furnace design will not improve the generated electromagnetic forces. The position of the coils is the limiting factor. If the distance between the coils and the center point of the crucible does not change, crucible size does not matter in the system. Therefore, the furnace should be adjusted accordingly.

In conclusion, this only provides a theoretical solution for the research problem. Different crucible sizes may be used in real-life applications other than the crucible size used in this study. The results should be compared with practical applications. It should be noted that carbon concentration and growth rate should be researched further for different crucibles. Those are mentioned for future work in the chapter 5.4.

5.3 Maximum Crucible Size

In the last section, it is mentioned that adjusting the crucible size has a significantly positive effect on the penetration of electromagnetic forces. However, bigger crystals are desired for most top-seeded solution growth applications. In order to find a good spot that includes good electromagnetic force penetration and the use of the biggest crucible possible, simulations were repeated with a gradually smaller crucible each time. In section 4.7, it is shown that a crucible with a diameter of 85 mm is the maximum crucible size that can be used with very high electromagnetic penetration for 500 Hz frequency. Since the original diameter was 100 mm, it is equivalent to a 15% reduction. Nearly all electromagnetic force domains reached the center with this amount of reduction in this application. This can be considered a good point while balancing electromagnetic force and penetration through the center. Bigger crucible sizes than that diameter will not have good penetration for 500 Hz frequency.

5.4 Future Work

In this research, the electromagnetic convection and the buoyancy convection in the silicon melt were analyzed for the SiC single crystal growth application that uses a TSSG furnace. As mentioned earlier in Section 3.5, the fluid flow has controlled mainly by 4 different convection mechanisms. This study is only focused on 2 convection mechanisms of 4 total. The remaining two mechanisms are Forced Convection and Marangoni Effect.

For further research, these two mechanisms should be included. Rotating the seed crystal or crucible itself causes forced convection because it physically moves the components. This may require very high computational power and time parameter for the simulation. Another convection mechanism is the Marangoni Effect which considers surface tension since there is an interface between the crucible and silicon melt. The free liquid surface of the silicon melt is assumed to be flat in this study. However, this is expected to contribute to fluid flow movement in a real-life application.

The temperature gradient is another important factor for solution growth applications. This can be implemented in the simulation with different software. In addition of temperature distribution in the crucible may make it easier to numerically calculate fluid flow movement. Very precise predictions can be done in this way. The study is completed in ANSYS software which allows the combination of different solvers that can be seen in Fig 5.1 below.

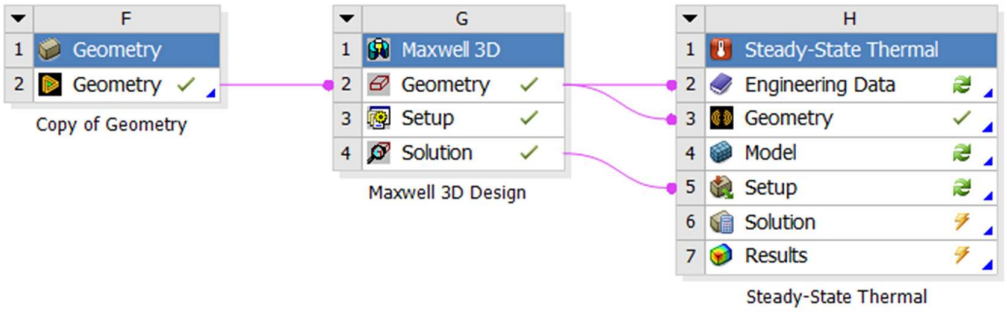

Figure 5.1: ANSYS Workbench Software that allows use simulations results further.

The outcome of this study can be taken to a steady-state thermal solver, and this will allow doing mentioned further research on this topic. The solution from simulations can be added as the parameter setup for the steady-state thermal solver by adding other parameters in the setup. Including all four convection mechanisms may be possible which can be used to make precise fluid flow movement calculations with the addition of temperature gradient to the system.

Appendix A

Simulation Setup

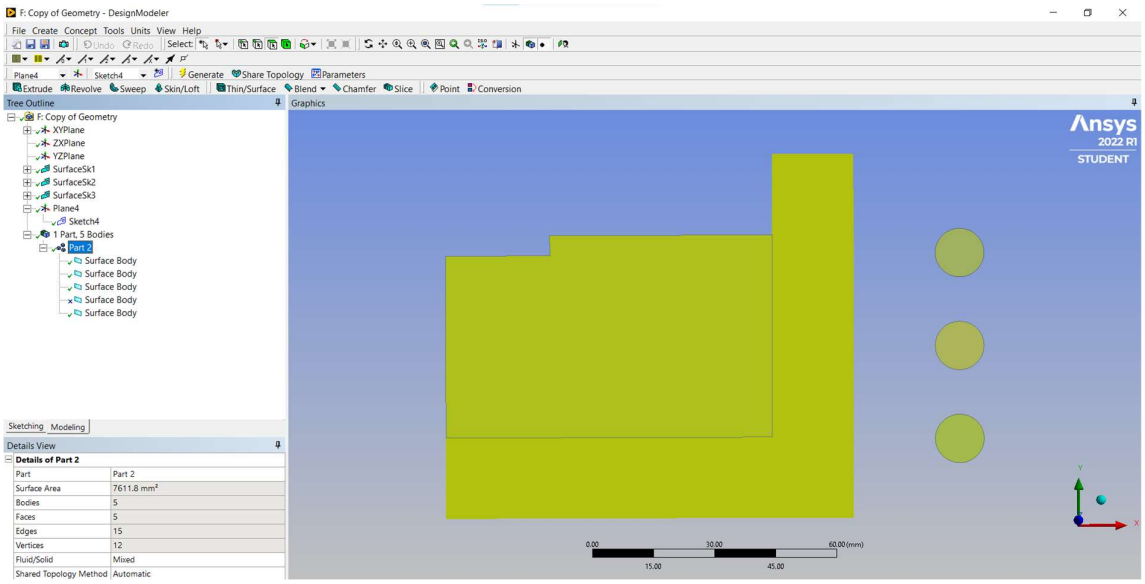

Figure A.1: Starting sketch in the ANSYS DesignModeler Software

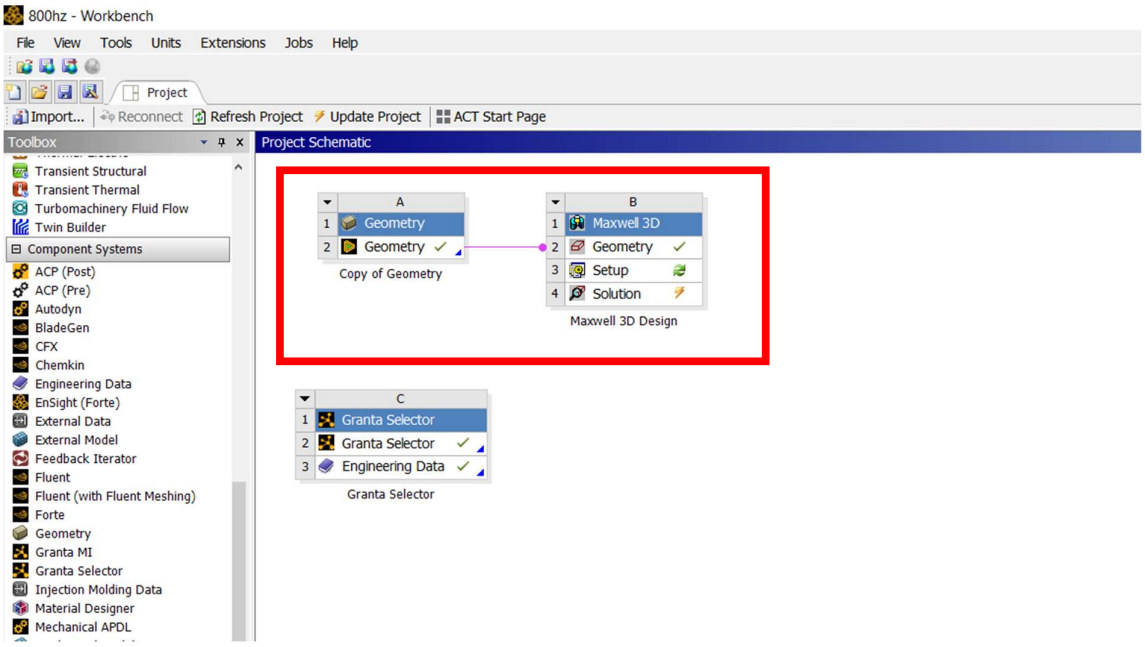

Figure A.2: Generated geometry in ANSYS DesignModeler software is connected to ANSYS Maxwell 3-D software

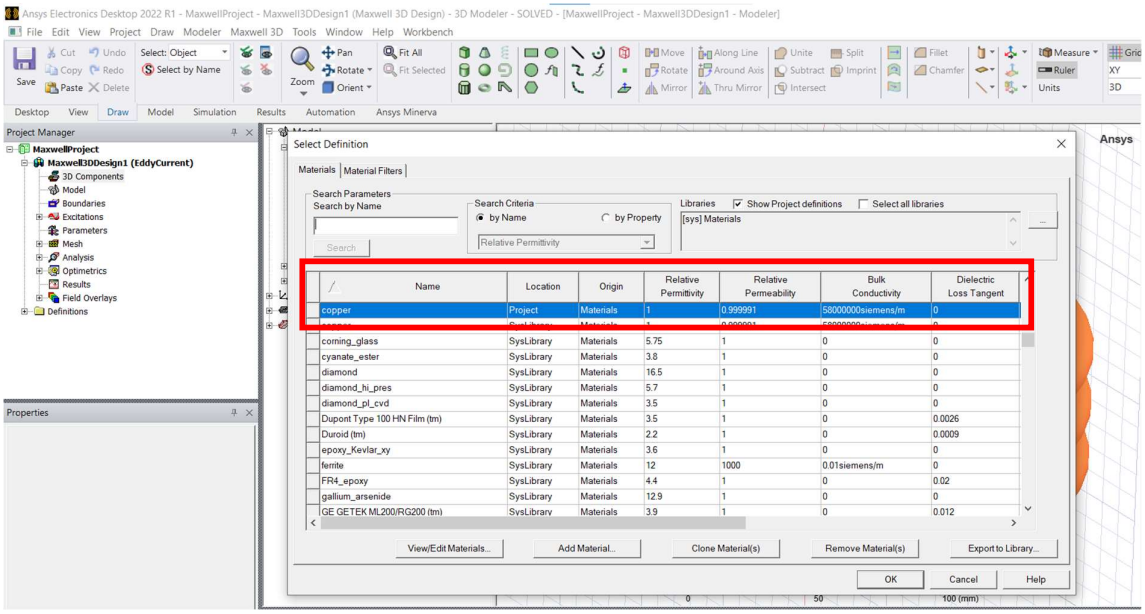

Figure A.3: Properties of copper used in coils

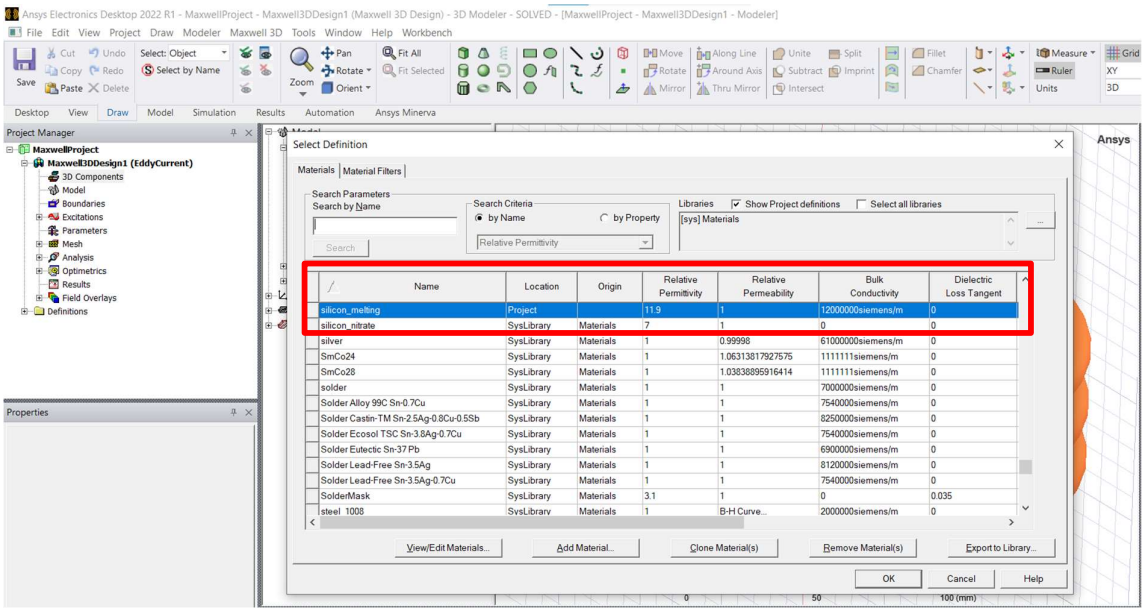

Figure A.4: Properties of silicon used in silicon melt

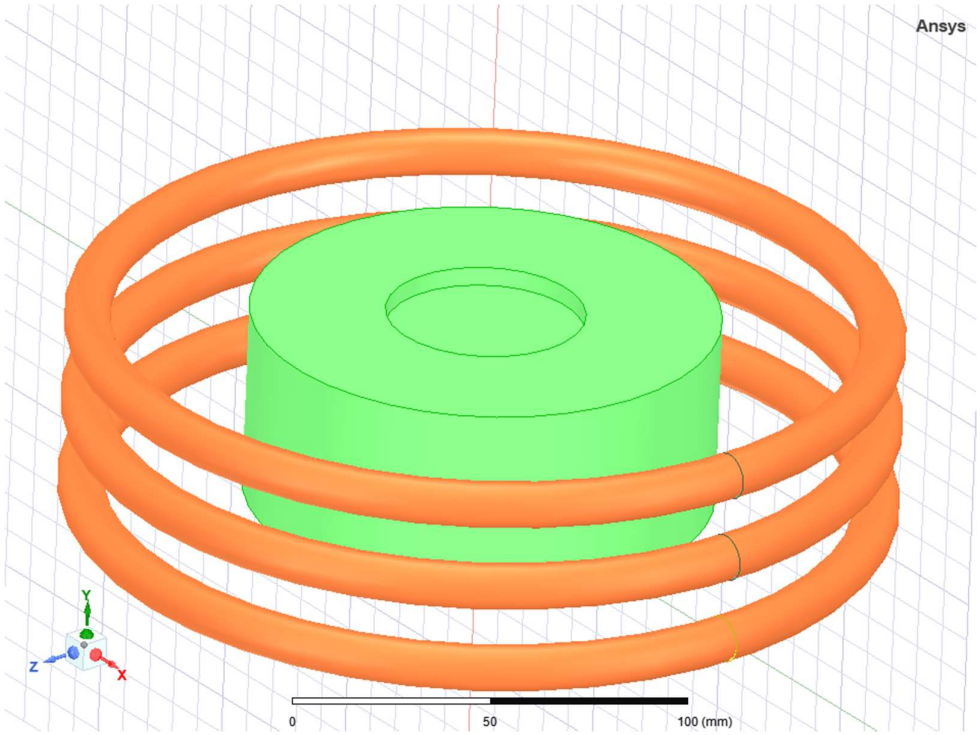

Figure A.5: Model used in the simulation (part in green is silicon melt, copper coils in orange)

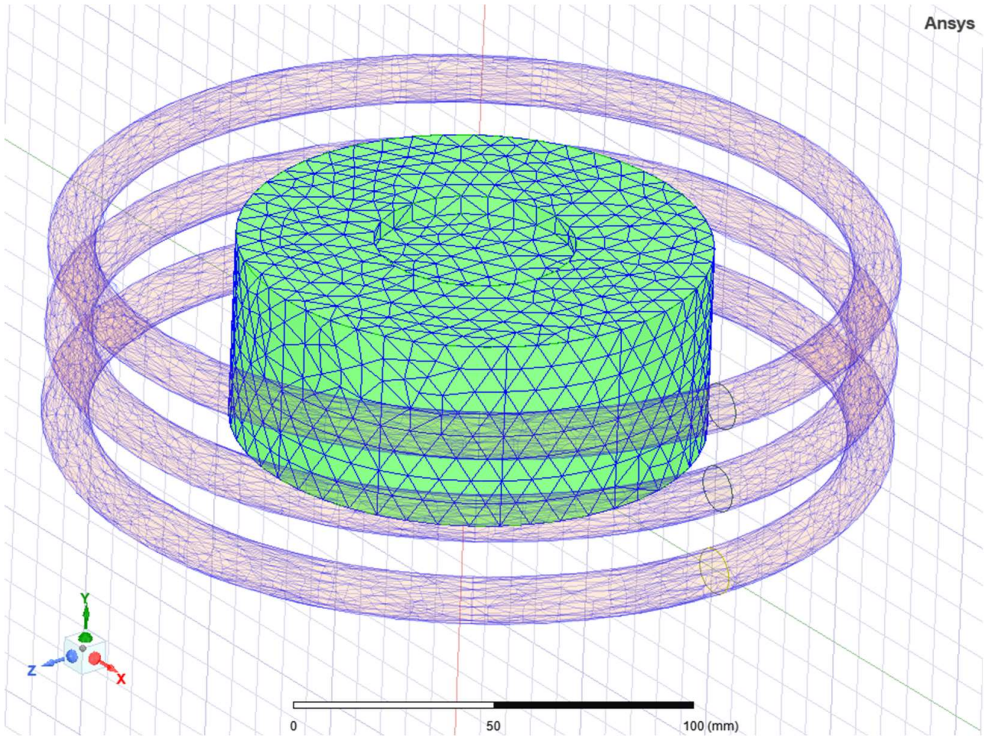

Figure A.6: Meshing of the model for numerical simulation

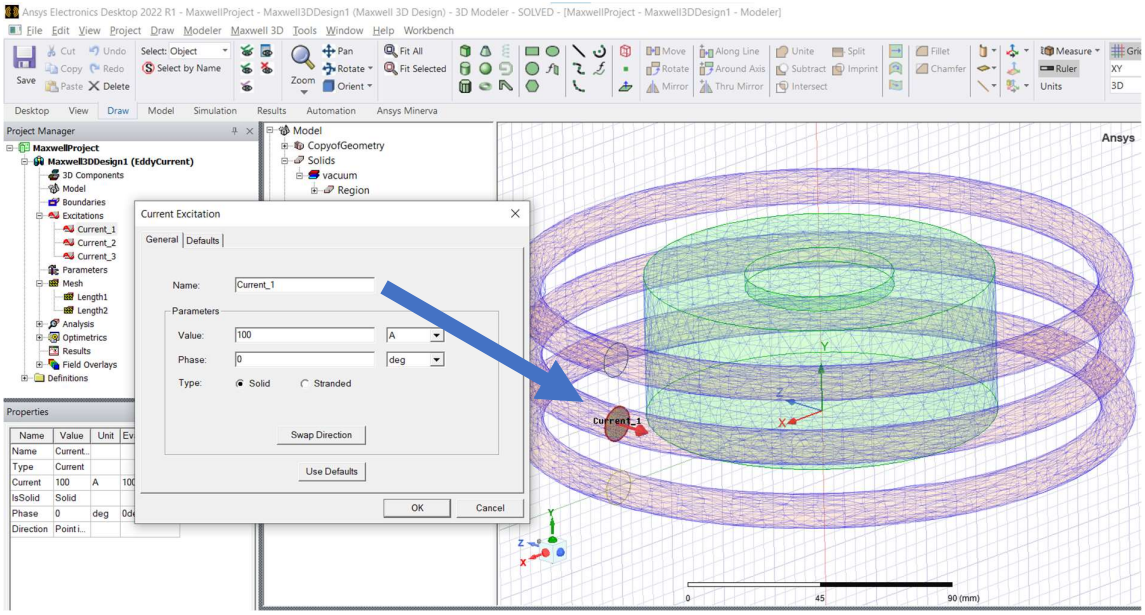

Figure A.7: Excitations for copper coils (current density of 100 Ampere, kept same for all simulations)

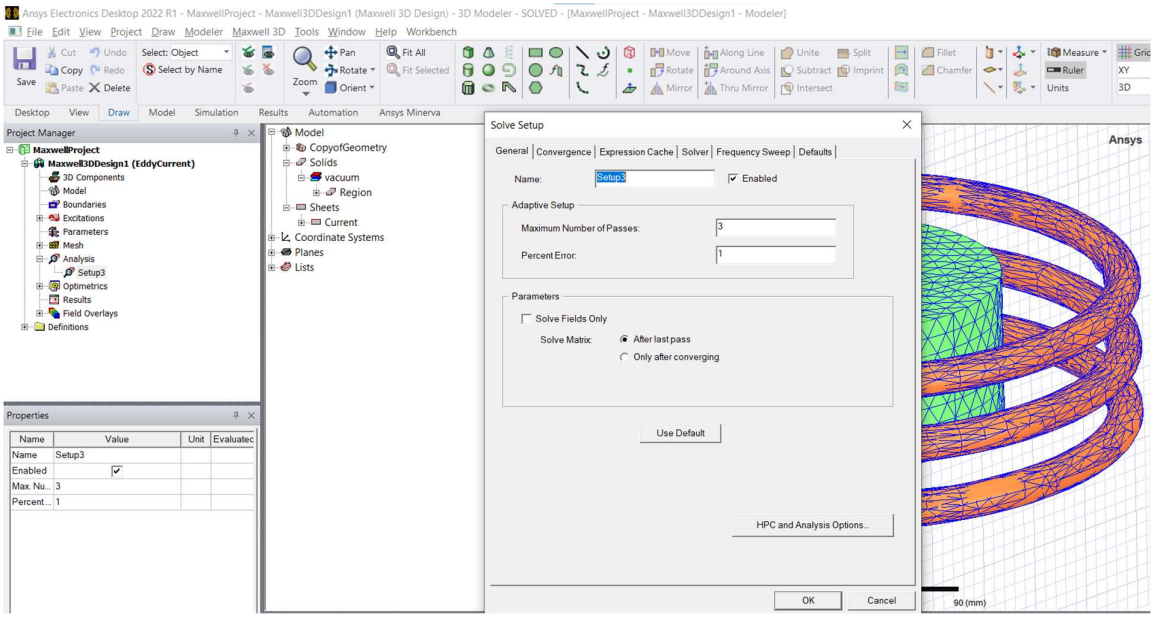

Figure A.8: General parameters for the setup

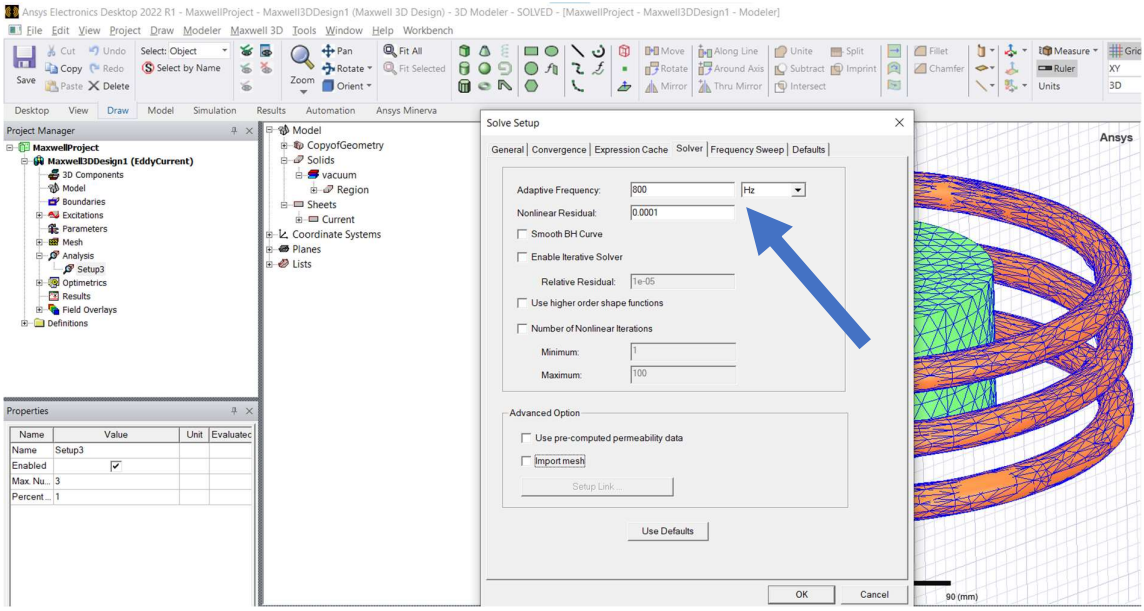

Figure A.9: Used frequency for the simulation setup (this is changed for all simulations)

References

1) I. Pritula , K. Sangwal, Fundamentals of crystal growth from solutions. In Handbook of crystal growth (pp. 1185-1227). Elsevier, 2015.

2) K. Seevakan, S. Bharanidharan, Different types of crystal growth methods. Int. J. Pure Appl. Math, 119, 5743-5758, 2018.

3) R. Falckenberg, The Verneuil Process. In: Goodman C.H.L. (eds) Crystal Growth., 109, 1978.

4) M. Sameed, Review of Structure, Properties and Fabrication of Single-Crystal Beryllium, 2010.

5) K. Sangwal, A novel self-consistent Nývlt-like equation for metastable zone width determined by the polythermal method. Crystal Research and Technology: Journal of Experimental and Industrial Crystallography, 44(3), 231-247, 2009.

6) V. Belruss, J. Kalnajs, A. Linz, R. C. Folweiler, Top-seeded solution growth of oxide crystals from non-stoichiometric melts. Materials Research Bulletin, 6(10), 899-905, 1971.

7) C. E. Miller, Method for growing single crystals of potassium niobate. Journal of Applied Physics, 29(2), 233-234, 1958.

8) L. Wang, T. Horiuchi, A. Sekimoto, Y. Okano, T. Ujihara, S. Dost, Three-dimensional numerical analysis of Marangoni convection occurring during the growth process of SiC by the RF-TSSG method. Journal of Crystal Growth, 520, 72-81, 2019.

9) D. Arivuoli, Principles of the Verneuil Growth Technique, Encyclopedia of Materials: Science and Technology, p. 7854-7856, 2001.

10) J. Friedrich, Methods for Bulk Growth of Inorganic Crystals: Crystal Growth, 5-13, 2016.

11) P. S. Dutta, Bulk Growth of Crystals of III–V Compound Semiconductors, 61-73, 2011.

12) P. E. Tomaszewski, Jan Czochralski—father of the Czochralski method, J. Cryst. Growth 236, 1–4, 2002.

13) D. Hurle, B. Cockayne, Czochralski growth, Handbook of crystal growth 2, 99–211, 1994.

14) B. Simon, R. Boistelle, Crystal growth from low temperature solutions. J. Cryst. Growth 52, 779–788, 1981.

15) H. J. Scheel, D. Elwell, Stable growth rates and temperature programming in flux growth, J. Cryst. Growth 12, 153-161, 1972.

16) Y. Tanaka, M. Matsuoka, Selection of solvents for organic crystal growth from solution J. Cryst. Growth 99, 1130–1133, 1990.

17) R. W. Olesinski, G. J. Abbaschian, The C-Si (Carbon-Silicon) system, Bulletin of Alloy Phase Diagrams 5, 486-489, (1984).

18) P. M. Gresho, J. J. Derby, J. Cryst. Growth 85, 40, 1987.

19) L. Wang, T. Horiuchi, A. Sekimoto, Y. Okano, T. Ujihara, S. Dost, Three-dimensional numerical analysis of Marangoni convection occurring during the growth process of SiC by the RF-TSSG method. J. Cryst. Growth 520, 72–81, 2020.

20) Q. Chen, Y. Jiang, J. Yan, M. Qin, Progress in modeling of fluid flows in crystal growth processes, Prog. Nat. Sci. 18, 1465–1473, 2008.

21) K. Ariyawong, Process modeling for the growth of SiC using PVT and TSSG methods, Université Grenoble Alpes, 2015.

22) A. Muiznieks, A. Krauze, B. Nacke, Convective phenomena in large melts including magnetic fields, J. Cryst. Growth 303 (2007) 211–220.